JOURNAL REVIEW

Density Functional Theory for Chemical Engineering: From Capillarity to Soft Materials

Jianzhong Wu
Dept. of Chemical and Environmental Engineering, University of California, Riverside, CA 92521

DOI 10.1002/aic.10713
Published online October 28, 2005 in Wiley InterScience (www.interscience.wiley.com).

Understanding the microscopic structure and macroscopic properties of condensed matter from a molecular perspective is important for both traditional and modern chemical engineering. A cornerstone of such understanding is provided by statistical mechanics, which bridges the gap between molecular events and the structural and physiochemical properties of macro- and mesoscopic systems. With ever-increasing computer power, molecular simulations and ab initio quantum mechanics are promising to provide a nearly exact route to accomplishing the full potential of statistical mechanics. However, in light of their versatility for solving problems involving multiple length and timescales that are yet unreachable by direct simulations, phenomenological and semiempirical methods remain relevant for chemical engineering applications in the foreseeable future. Classical density functional theory offers a compromise: on the one hand, it is able to retain the theoretical rigor of statistical mechanics and, on the other hand, similar to a phenomenological method, it demands only modest computational cost for modeling the properties of uniform and inhomogeneous systems. Recent advances are summarized of classical density functional theory with emphasis on applications to quantitative modeling of the phase and interfacial behavior of condensed fluids and soft materials, including colloids, polymer solutions, nanocomposites, liquid crystals, and biological systems. Attention is also given to some potential applications of density functional theory to material fabrications and biomolecular engineering. © 2005 American Institute of Chemical Engineers *AIChE J,* 52: 1169–1193, 2006
Keywords: statistical mechanics, complex fluids, thermodynamics/statistical, surface chemistry/physics

Introduction

The goal of statistical mechanics is to interpret and predict the properties of macroscopic systems on the basis of their microscopic constituents.[1,2] It provides the bedrock for understanding numerous natural phenomena and for design and optimization of chemical processes. The importance of statistical mechanics in chemical engineering has been recognized for many years.[3-5] One prominent example, primarily from the 1960s and 1970s, is the development and application of equations of state and local-composition models, attained by ingenious combinations of basic concepts from statistical mechanics (in particular, van der Waals equation of state and Boltzmann's distribution law) with extensive experimental data.[6,7] These semiempirical methods have been widely used in phase- and chemical-equilibrium calculations that are essential in chemical engineering practice. Another well-known example constitutes the applications of statistical-mechanical models to gas adsorption and hydrate formation.[8,9]

Although the van der Waals equation of state and Boltzmann's distribution law have played a pivotal role in many classical molecular-thermodynamic models, in recent years, a

Correspondence concerning this article should be addressed to J. Wu at jwu@engr.ucr.edu.

number of more sophisticated statistical-mechanical methods have also been used, driven by diverse special applications related to fluid-phase equilibria, polymeric materials, colloids, and interfacial engineering. These more rigorous theoretical methods are based on molecular simulations,[10,11] liquid-state theories,[12,13] polymer self-consistent field theory,[14-16] and classical density functional theory.[17,18] For example, powerful field-theoretical methods have been developed for predicting the mesoscopic structures of polymeric systems;[14] general equations of state have been established for fluid-phase equilibrium calculations involving virtually any system of practical interest.[19,20] With the rapid increase of computer power, molecular simulation and *ab initio* quantum mechanics promise to offer a universal approach to the realization of the full potential of statistical mechanics.[21] However, simulation cannot replace all analytical methods in the near future, not only because significant progress has yet to be made for modeling multiple time- and length-scale problems that cannot be described by current simulation methods but, more important, interpretation of simulation data, much like experimental results, often requires analytical tools to attain a good understanding of the underlying physics. Analytical methods are by and large much more efficient than direct simulations for predicting the molecular constituents of a system with "tailored" properties, a reverse problem that is of much interest in practical applications including drug design, gene mutation, and materials synthesis.

Classical *density functional theory* (DFT) provides a compromise between conventional semiempirical methods and molecular simulations.[18,22-24] On the one hand, DFT is able to retain the microscopic details of a macroscopic system at a computational cost significantly lower than that used in simulation methods. On the other hand, DFT is more rigorous than conventional phenomenological theories. It is applicable to both uniform and confined systems within a self-consistent theoretical framework. Although the practical value of DFT for modeling interfacial properties was recognized soon after the methodology was first introduced to classical systems in 1976,[25] its broader applications for studying equilibrium and kinetics of phase transitions, self-assembly, properties of polymeric materials, thin films, and a variety of biological systems emerged only recently. Meanwhile, much progress has been made in recent years in the development of more efficient numerical algorithms and in the formulation of more realistic free-energy functionals to account for the thermodynamic nonideality attributed to various intermolecular forces.

The purpose of this article is to review, along with illustrative examples, recent progress of classical DFT in modeling the phase and interfacial properties of fluids and soft materials. Following a brief introduction to the basic concepts and new developments toward a unified free-energy functional reflecting various components of intermolecular forces, the main text is concerned with applications of DFT to (1) surface tension and interfacial behavior, (2) adsorption of gas and materials characterization, (3) wetting transitions, (4) solvation, (5) freezing and melting transitions, (6) phase behavior of liquid crystals, (7) properties of polymeric materials and composites, and (8) molecular self-assembly. This article concludes with a brief discussion of some possible future applications of DFT to fabrication of novel materials, environmental protection, and biomolecular engineering.

No attempt has been made to cover all aspects of classical DFT in the recent literature. Therefore, significant publications may have been omitted. The contents discussed here are illustrative rather than exhaustive. Topics of interest to chemical engineers that are not discussed because of the page limitation include transport in ion channels,[26,27] properties of biomacromolecular molecules in a "crowded" environment,[28] kinetics of nucleation,[29] and nonequilibrium phase transitions.[30-32] A review of these topics would show that DFT is useful not only for solving equilibrium problems but also for modeling kinetics and transport phenomena at the molecular level.

Classical Density Functional Theory (DFT)

Basic concepts

Classical DFT stems from *a mathematical theorem* stating that in an open system specified by temperature T, total volume V, and chemical potentials of all constituent molecules μ_i, the underlying external potential for each chemical species, denoted by $\psi_i(\mathbf{R})$, is *uniquely* determined by the equilibrium density profiles or by the spatial distribution of molecules $\rho_i(\mathbf{R})$.[33] A corollary of this theorem is that for a classical system, the Helmholtz energy can be expressed as a unique functional* of the density profiles of the constituent molecules, independent of the external potential. This Helmholtz energy functional, designated as $F[\rho_i(\mathbf{R})]$, is often referred to as the *intrinsic Helmholtz energy*, meaning that it is an inherent property of the system and is independent of the external potential. The mathematical foundation of DFT, in the language of quantum mechanics, was first established by Hohenberg and Kohn[33] in a seminal article published in 1964 concerning the ground-state properties of an electron gas. It was later generalized to nonzero temperatures by Mermin.[34] Indeed, from a mathematical perspective, classical DFT closely resembles electronic DFT (unfortunately both have the same acronym) except that in the former case, the density functional applies to the structure of atoms or coarse-grained elements of a polymeric molecule, whereas the latter applies to electrons. Fueled with a pragmatic computational scheme proposed by Kohn and Sham,[35] electronic DFT has evolved into a powerful approach in computational chemistry.

Although in a classical sense, the position of an electron or atom can be specified by a conventional three-dimensional vector $\mathbf{r}$, a vector of higher dimensionality is necessary to describe the spatial configuration of a polyatomic molecule with m atoms (see Figure 1). A molecular density profile $\rho_i(\mathbf{R})$ is thus defined as the ensemble average of instantaneous molecular densities

$$\rho_i(\mathbf{R}) = \left\langle \sum_{N_i} \delta(\mathbf{r}_1, \mathbf{r}_2, \ldots, \mathbf{r}_{m_i}) \right\rangle \tag{1}$$

where the multidimensional vector $\mathbf{R} = (\mathbf{r}_1, \mathbf{r}_2, \ldots, \mathbf{r}_m)$ denotes the positions of all atomic particles; N_i stands for the number of molecules of species i; and δ represents a multidimensional Dirac-delta function, which is infinite when m atoms

* A *functional* is a function whose input variable is also a function. For instance, in a simple atomic fluid the Helmholtz energy functional $F[\rho(\mathbf{r})]$ maps a density function $\rho(\mathbf{r})$ to a real number for the Helmholtz energy.

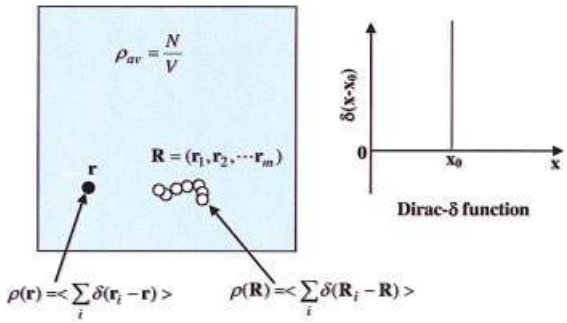

Figure 1. Definitions of the average molecular density ρ_{av}, average local atomic density $\rho(\mathbf{r})$, and average local molecular density $\rho(\mathbf{R})$ in a system consisting of N polyatomic molecules in volume V.

The instantaneous density of an atom i at position $\mathbf{r}$ is specified by a three-dimensional Dirac-δ function $\delta(\mathbf{r} - \mathbf{r}_i)$. Similarly, the instantaneous density of a molecule i with m atoms is specified by a $3m$-dimensional Dirac-δ function $\delta(\mathbf{R} - \mathbf{R}_i)$, where $\mathbf{R} = (\mathbf{r}_1, \mathbf{r}_2, \ldots, \mathbf{r}_m)$ is a $3m$-dimensional vector. The angle brackets stand for ensemble averages. As illustrated, a Dirac-δ function $\delta(\mathbf{x} - \mathbf{x}_0)$ is everywhere zero except that at a specific position $(\mathbf{x}_0)$, it is infinite. The Dirac-δ function satisfies the normalization condition $\int d\mathbf{x}\delta(\mathbf{x} - \mathbf{x}_0) = 1$. [Color figure can be viewed in the online issue, which is available at www.interscience.wiley.com.]

of the polyatomic molecule are placed at $\mathbf{R} = (\mathbf{r}_1, \mathbf{r}_2, \ldots, \mathbf{r}_{m_i})$ and zero otherwise. The angle brackets in Eq. 1 stand for the ensemble average. Because the multidimensional vector $\mathbf{R}$ defines not only the position but also the configuration or spatial arrangement of a multiatomic molecule, the molecular density profile $\rho_i(\mathbf{R})$ entails information on both the microscopic structure and on the average configuration of molecules.

For convenience, the multidimensional molecular density $\rho_i(\mathbf{R})$ is often expressed in terms of the atomic densities $\rho_{i,j}(\mathbf{r})$, that is, the density profiles of the consisting atomic particles,

$$\rho_{i,j}(\mathbf{r}) = \int d\mathbf{R}\delta(\mathbf{r} - \mathbf{r}_j)\rho_i(\mathbf{R}) \tag{2}$$

where the subscript j stands for an atom and the subscript i for a molecule. If concern is restricted to atomic fluids such as argon, the molecular density is simply a function of a normal three-dimensional vector standing for the position of an atom. Even though, in a uniform atomic fluid, the spatial average of the atomic density $\rho(\mathbf{r})$ becomes identical to the bulk density ρ_{av}, the local density $\rho(\mathbf{r})$ can be infinitely large when the atoms are localized such as in an idealized crystalline solid. For example, in a one-component hard-sphere system at the close-packed limit, the average reduced density is $\rho_{av}\sigma^3 = \sqrt{2}$, where σ denotes the hard-sphere diameter. In this case, the hard spheres are arranged onto a face-centered cubic lattice and the local density is infinite at the lattice sites and zero otherwise.

The *second law of thermodynamics* requires that, for an open system, the grand potential Ω must be minimized at equilibrium. The grand potential is also a functional of the molecular density $\rho_i(\mathbf{R})$, defined as

$$\mathbf{\Omega}[\rho_i(\mathbf{R})] = F[\rho_i(\mathbf{R})] + \sum_i \int d\mathbf{R}\rho_i(\mathbf{R})[\psi_i(\mathbf{R}) - \mu_i] \tag{3}$$

Minimization of the grand potential functional yields a variational equation

$$\delta F[\rho_i(\mathbf{R})]/\delta\rho_i(\mathbf{R}) + \psi_i(\mathbf{R}) - \mu_i = 0 \tag{4}$$

Given an expression for the intrinsic Helmholtz energy functional $F[\rho_i(\mathbf{R})]$, Eq. 4 can be solved to obtain the equilibrium density profiles. From these density profiles, both structural and thermodynamic properties of the system can be calculated by following the standard statistical–mechanical relations.[2] The detail formalism of DFT can be found in textbooks and previous reviews.[17,18]

DFT is useful not only for inhomogeneous systems that are subject to an external field but also for uniform systems such as conventional bulk vapor and liquid phases, and for anisotropic fluids such as liquid crystals. Although the average local density of a uniform fluid is the same everywhere, near an arbitrary tagged molecule the average local density is inhomogeneous. Indeed, as shown in Figure 2, this local average density is closely related to the structure of a fluid or to the radial distribution function. It has been demonstrated that DFT can be used to derive various liquid-state theories including the Ornstern–Zernike equation and its closures such as that using hypernetted chain (HNC) theory.[22]

Landmarks of classical DFT

Apart from the aforementioned mathematical theorem, variational approaches were used in statistical mechanics long before the advent of classical DFT. As early as 1893, van der Waals developed a successful molecular theory for representing the structure and surface tension of a vapor–liquid interface. Van der Waals' theory is based on a gradient expansion of the Helmholtz energy functional with respect to a conjectured interfacial density profile[36]

$$F = \int d\mathbf{r}\Phi[\rho(\mathbf{r})] + \kappa \int d\mathbf{r}[\nabla\rho(\mathbf{r})]^2 \tag{5}$$

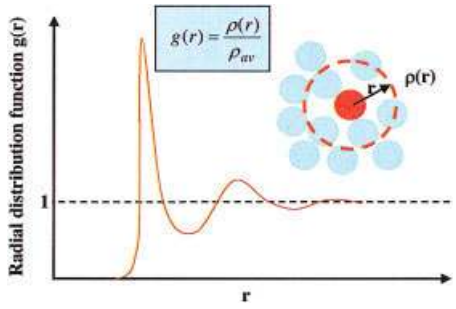

Figure 2. DFT is applicable to both uniform and inhomogeneous systems.

Even in a uniform fluid such as liquid argon, the average local density near an arbitrarily tagged molecule is inhomogeneous. The ratio of the local density $\rho(r)$ and the average density ρ_{av} defines a radial distribution function, an important quantity for describing the microscopic structure. A similar concept can be applied to polyatomic systems to define intra- and intermolecular correlation functions.[278,279] [Color figure can be viewed in the online issue, which is available at www.interscience.wiley.com.]

where $\Phi(\rho)$ is the Helmholtz energy density of the corresponding uniform fluid with a molecular number density ρ, and κ is a constant related to the Boltzmann constant k_B and the direct correlation function $c(r, \bar{\rho})$** at an average density $\bar{\rho} = (\rho_L + \rho_V)/2$ of the coexisting vapor and liquid phases

$$\kappa = \frac{k_B T}{12} \int d\mathbf{r} r^2 c(r, \bar{\rho}) \tag{6}$$

Regrettably, van der Waals' important work was not widely recognized until it was reinvented first by Landau and Lifshitz in 1935, to describe the boundary of two magnetic domains; and later by Mitsui and Furuichi in 1953, for studying the interface between two ferroelectric structures; and most notably by Cahn and Hilliard in 1958, to represent the structure and surface tension of vapor–liquid as well as liquid–liquid interfaces.[37] The later versions of van der Waals' square-gradient theory remain useful in many aspects of modern physics and engineering applications, particularly for understanding the interfacial properties of fluids.

Another prominent variational approach in statistical mechanics was introduced by Onsager in 1949 for modeling the isotropic–nematic transition of lyotropic liquid crystals.[†38] For a system consisting of nonspherical rigid particles, the molecular density profile $\rho(\mathbf{R})$ can be expressed in terms of the center of mass $\mathbf{r}$ and orientation angle ω of liquid-crystal molecules, that is, $\rho(\mathbf{R}) = \rho(\mathbf{r}, \omega)$. Based on the lowest-order expansion of the Helmholtz energy functional in terms of the anisotropic density profile, Onsager derived

$$F = \int d\mathbf{r} d\omega \rho(\mathbf{r}, \omega)[\ln \rho(\mathbf{r}, \omega) - 1] - \frac{k_B T}{2} \int d\mathbf{r}_1 d\omega_1 \int d\mathbf{r}_2 d\omega_2 \rho(\mathbf{r}_1, \omega_1)\rho(\mathbf{r}_2, \omega_2) f(\mathbf{r}_1 - \mathbf{r}_2, \omega_1, \omega_1) \tag{7}$$

where $f = e^{-\beta u} - 1$ is the Mayer function, $\beta = 1/(k_B T)$, and u stands for the pair potential between the anisotropic molecules. The first term on the right-hand side of Eq. 7 represents the Helmholtz energy functional of noninteracting (ideal) rigid particles, and the second term represents the contribution arising from the intermolecular interactions, obtained from the virial expansion of the Helmholtz energy functional truncated at the second-order level. Onsager's theory forms a foundation for later theoretical developments and remains popular for understanding the structure and interfacial behavior of liquid crystals.[39] Conceptually, it is essentially the same as the virial expansion for the equation of state of a nonideal gas.

The first application of DFT as a general methodology to classical systems was introduced by Ebner, Saam, and Stroud in 1976 for modeling the interfacial properties of a Lennard–Jones (LJ) fluid.[25] Similar to van der Waals' square-gradient theory, the intrinsic Helmholtz energy functional was derived from a partial summation of the gradient expansion

$$F = \int d\mathbf{r} \Phi[\rho(\mathbf{r})] + \frac{k_B T}{4} \int d\mathbf{r}_1 d\mathbf{r}_2 c(|\mathbf{r}_1 - \mathbf{r}_2|; \bar{\rho})[\rho(\mathbf{r}_1) - \rho(\mathbf{r}_2)]^2 \tag{8}$$

where $c(r, \bar{\rho})$ stands for the direct correlation function of a uniform bulk fluid with a density $\bar{\rho} = [\rho(\mathbf{r}_1) + \rho(\mathbf{r}_2)]/2$. It was demonstrated that Eq. 8 provides a good description of the vapor–liquid surface tensions and the interfacial density profiles of argon over a wide range of temperatures. Aside from its theoretical implications, the most significant part of this work is the prediction of a first-order prewetting transition of unsaturated argon gas at the surface of solid carbon dioxide. Although a similar prewetting transition was independently predicted by Cahn following van der Waals' square-gradient theory,[40] the novel phase behavior stood for more than a decade without experimental support and provoked much heated controversy. Experimental verification of the prewetting transition was first reported about 15 years later by Rutledge and Taborek for adsorption of helium on cesium at extremely low temperatures.[41]

Excess Helmholtz energy functional

Whereas the mathematical framework of DFT is formally exact, a precise expression of the intrinsic Helmholtz energy as a functional of the molecular density profiles is unknown for most systems of practical interest.[††] Formulation of the Helmholtz energy functional is a task essentially equivalent to enumeration of the statistical partition function for the particular system under investigation. A viable approach, practiced in classical thermodynamics for more than 100 years, is to divide the Helmholtz energy into an ideal part and an excess part. The ideal part represents the contribution of an ideal gas where all nonbonded interactions are turned off; the excess part accounts for interactions leading to the thermodynamic nonideality.

For an ideal-gas system that is free of nonbonded interactions, the Helmholtz energy functional is known exactly:

$$F^{id} = \sum_i k_B T \int d\mathbf{R} \rho_i(\mathbf{R})[\ln \rho_i(\mathbf{R}) - 1] + \sum_i \int d\mathbf{R} \rho_i(\mathbf{R}) V_i(\mathbf{R}) \tag{9}$$

where $V_i(\mathbf{R})$ stands for the bond potential of a molecule i with all its segments connected in a configuration $\mathbf{R}$. Because of the multidimensional integrals on the right-hand side of Eq. 9, it is not simple by any means to evaluate the ideal Helmholtz energy functional analytically. Nevertheless, it is in a closed form and the thermodynamic properties of this ideal system can

** Mathematically, a direct correlation function is defined as a second functional derivative of an excess Helmholtz energy functional with respect to density profiles. As discussed later, the excess Helmholtz energy functional is the Helmholtz energy functional of the system under consideration minus that of an ideal-gas system at the same temperature and density profiles.

† Although the definitions of lyotropic and thermotropic liquid crystals vary from text to text, in this article, the former refers to an athermal system, such as hard rods or ellipsoids, and the latter is a system in which the thermodynamic properties depend on both concentration and temperature.

†† One notable exception is hard rods and hard-rod mixtures in one dimension.

be easily calculated using a modern computer, even for systems containing molecules of arbitrary topology. The bond potential that appeared in Eq. 9 may include contributions resulting from bond stretching, angle bending, and torsional terms.[42]

The excess part of the Helmholtz energy functional, designated as F^{ex}, is unknown for most systems of practical interest. However, it can be approximately formulated by following rigorous mathematical analysis and, more important, by physical insights for the specific system under consideration. Because F^{ex} arises from the nonbonded interactions between atomic segments, we may make a variational ansatz that the excess Helmholtz energy can be expressed as a functional depending only on the atomic density profiles, that is,

$$F^{ex}[\rho_i(\mathbf{R})] = F^{ex}[\rho_{i,1}(\mathbf{r}), \rho_{i,2}(\mathbf{r}), \ldots, \rho_{i,m_i}(\mathbf{r})] \qquad (10)$$

Equation 10 is formally exact as long as $F^{ex}[\rho_{i,1}(\mathbf{r}), \rho_{i,2}(\mathbf{r}), \ldots, \rho_{i,m_i}(\mathbf{r})]$ includes the multibody correlations of atomic segments arising from bond connectivity. In other words, $F^{ex}[\rho_{i,1}(\mathbf{r}), \rho_{i,2}(\mathbf{r}), \ldots, \rho_{i,m_i}(\mathbf{r})]$ should be different from that for an atomic system (where all chemical bonds are removed) even when they have the same density profiles. It is important to notice that the bonding potential does not enter directly into the formulation of $F^{ex}[\rho_{i,1}(\mathbf{r}), \rho_{i,2}(\mathbf{r}), \ldots, \rho_{i,m_i}(\mathbf{r})]$.

Because the nonbonded interatomic forces are conventionally expressed in terms of short-range repulsion, van der Waals attraction, electrostatic forces, electron donor–acceptor interactions, and so on, each component of the intermolecular potential makes a distinct (but not necessarily independent) contribution to $F^{ex}[\rho_{i,1}(\mathbf{r}), \rho_{i,2}(\mathbf{r}), \ldots, \rho_{i,m_i}(\mathbf{r})]$. In principle, one may derive a unified expression describing all components of the intermolecular forces (bonded and nonbonded) from quantum mechanics. In that case, an accurate expression for the excess Helmholtz energy functional would allow us to develop a unified DFT applicable to all molecular systems. Although the same argument can be used for molecular simulations, the advantages of DFT are clear: DFT focuses on the direct connection between free energy and molecular structure (density profiles) rather than on the overwhelming data generated by the trajectories of all constituent particles in molecular simulation. A microscopic state of a many-body system entails $6N$ degrees of freedom (where N is the number of spherical particles in the system), whereas the density of a spherical object is a simple function that depends solely on the three-dimensional vector $\mathbf{r}$. Therefore use of DFT provides deeper insights into the underlying physics of natural phenomena and, more important, reduces the computational demands.

Elements of nonideality

Short-range Repulsion. In statistical mechanics, the short-range repulsion between two atomic particles (atoms or coarse-grained elements of a polymer) is often represented by the hard-sphere model, which assumes that each particle has a physical volume prohibiting an overlap with other particles. This excluded-volume effect plays a central role in determining the structure and thermodynamic properties of condensed materials. It has been long recognized that, with an analytical theory for hard spheres, the thermodynamic nonideality arising from other components of the intermolecular forces can be included by perturbation expansions of the Helmholtz energy functional with respect to either the density profile or the intermolecular potential.[43]

The structure and thermodynamic properties of a bulk hard-sphere fluid can be accurately described by various analytical theories, that is, the scaled-particle theory,[44] Percus–Yevick equation,[45] and Boublik–Mansoori–Carnahan–Starling–Leland (BMCSL) equation of state.[46,47] Over the past two decades, numerous versions of DFT have been published for representing the structure and thermodynamic properties of inhomogeneous hard spheres (see Evans[22] and Cuesta et al.[48] for the literature before 1992 and for the developments made over the past decade, respectively). Among them, the fundamental measure theory (FMT), first proposed by Rosenfeld,[49] bears a number of special features. First, this geometry-based DFT is built on firm physical and mathematical foundations rather than on empirical approximations. Unlike alternative versions of DFT for hard spheres that apply weighted density approximations, FMT does not require the bulk properties of hard spheres as input; instead, it can be reduced to a theory of bulk fluids as an output. Theoretically, FMT provides an exact dimensional crossover, that is, it is equally applicable to bulk systems (3D), hard spheres confined between surfaces (2D), in a cylindrical pore (1D), and in a cavity (0D). It is a self-consistent theory directly applicable to one component and polydisperse mixtures, fluid and solid phases, and systems consisting of nonspherical particles including liquid crystals.[50] From a practical perspective, it performs well at all densities, particularly at high densities where alternative methods are inappropriate.

A number of modifications of FMT have been proposed since it was first published in 1989.[48] Because the accuracy of FMT is similar to that of the scaled-particle theory or Percus–Yevick theory for bulk hard spheres,[51] its numerical performance can be further improved by using the quasi-exact BMCSL equation of state for bulk hard-sphere fluids.[52,53] According to this version of FMT, the excess Helmholtz energy functional can be expressed in terms of four scalar and two vector-weighted densities, as introduced by Rosenfeld,[49]

$$F_{hs}^{ex} = k_B T \int d\mathbf{r} \left\{ -n_0 \ln(1-n_3) + \frac{n_1 n_2 - \mathbf{n_{V1}} \mathbf{n_{V2}}}{1-n_3} + \frac{1}{36\pi} \left[n_3 \ln(1-n_3) + \frac{n_3^2}{(1-n_3)^2} \right] \frac{(n_2^3 - 3n_2 \mathbf{n_{V2}} \mathbf{n_{V2}})}{n_3^3} \right\} \qquad (11)$$

where $\{n_\alpha\}$ stand for the weight functions that are related to the geometry of a spherical particle, that is, the center of mass, surface area, and volume. For a uniform fluid, the vector-weighted densities disappear and Eq. 11 reduces to the excess Helmholtz energy from the BMCSL equation of state. Although the modified FMT preserves most advantages of the original theory, it improves the numerical performance, particularly for highly asymmetric hard-sphere systems.

Van der Waals Attraction. In addition to short-range repulsion, van der Waals' attraction is another essential component of nonbonded interatomic interactions. Most versions of DFT take a mean-field approach to account for the contribution of van der Waals forces to the excess Helmholtz energy functional. Although results from the mean-field approximation may capture some essential features arising from the attractive forces, they are at most semiquantitative, as one may anticipate

from the van der Waals equation of state. A first step toward an improvement is by a quadratic density expansion of the excess Helmholtz energy functional relative to that for a uniform fluid:[54]

$$F_{att}^{ex} = F_{att}^{ex}(\rho_i^0) + \sum_i \mu_i^{att} \int d\mathbf{r}\Delta\rho_i(\mathbf{r}) - \frac{k_BT}{2}\sum_{i,j}\iint d\mathbf{r}d\mathbf{r}' c_{ij}^{att}(|\mathbf{r}-\mathbf{r}'|)\Delta\rho_i(\mathbf{r})\Delta\rho_j(\mathbf{r}') \quad (12)$$

where $F_{att}^{ex}(\rho_i^0)$ is the attractive part of the excess Helmholtz energy of the reference bulk fluid and ρ_i^0 is the average density of an atomic component i. This "semiquadratic" approach requires the excess chemical potential μ_{att}^{ex} and the direct correlation function $c_{ij}^{att}(\mathbf{r})$ of a uniform atomic fluid as input. For that purpose, the analytical correlation functions derived from the first-order mean-spherical approximation (FMSA) are particularly useful.[55-60] It has been demonstrated that, at least for relatively simple models such as Lennard–Jones systems and coarse-grained models of polymers, excellent agreement between theory and simulation results can be attained.[61] Because the analytical expressions of both the excess chemical potentials and direct correlation functions are readily available from FMSA, the numerical implementation and computational cost of the quadratic approximation are very comparable to those for a mean-field approach.

Weak Association. Another important component in a conventional force field is the formation of chemical or hydrogen bonds as in associating fluids. For fluid-phase equilibrium calculations, the thermodynamic perturbation theory[62,63] has been successfully used to develop the statistical associating fluid theory (SAFT), a generic equation of state for associating fluids and also for polymers.[64] By incorporation of basic concepts from DFT, various extensions of SAFT have been applied to inhomogeneous associating fluids near a hard wall, in slit pores, and at vapor–liquid or liquid–liquid interfaces.[65-73] A relatively simple version of the excess Helmholtz energy functional was recently derived by introducing the scalar- and vector-weighted densities of FMT into the SAFT equation of state:

$$F_{ass}^{ex} = k_BT\sum_{i,A}\int dr n_0\zeta_i[\ln X_i^{(A)} - X_i^{(A)}/2 + 1/2] \quad (13)$$

where the subscript i stands for the atomic species i with the association site A. The inhomogeneous factor ζ_i is related to Rosenfeld's weighted densities by

$$\zeta_i = 1 - \mathbf{n}_{\mathbf{V2},i}\cdot\mathbf{n}_{\mathbf{V2},i}/n_{2,i}^2 \quad (14)$$

and $X_i^{(A)}$ is the local fraction of i not bonded at an associating site A. It has been demonstrated that Eqs. 13 and 14 provide a quantitative description of chemical bonding for inhomogeneous associating fluids including waterlike molecules.[68]

Electrostatics. For systems with Coulomb interactions, a common DFT approach uses a quadratic density expansion of the Helmholtz energy functional with respect to that of a bulk fluid or a suitably chosen, position-dependent reference fluid.[74-78] Similar to Eq. 12, the direct correlation functions in this "semiquadratic" expansion are obtained from an integral-equation theory, mostly from the analytical solutions of the mean-spherical approximation (MSA).[79] Unlike various mean-field theories derived from the Poisson–Boltzmann (PB) equation, the quadratic approximation is often sufficient to capture a number of counterintuitive electrostatic phenomena observed in solutions containing multivalent ions such as charge inversion of macroions and attraction between like charges.[80,81] The limitation of the PB equation arises from its neglect of the size of small ions and the correlation of charge distributions.

Correlations Attributed to Chain Connectivity. Application of classical DFT to polymeric systems was first discussed by Chandler, McCoy, and Singer (CMS) in 1986.[82] The past few years have witnessed enormous growth in this area.[83-88] Early versions of polymer DFT were heavily influenced by the self-consistent field theory and by Landau expansions for the selection of the reference system or for the formulation of the free-energy functional. These influences remain evident in different versions of dynamic DFT.[14,30] Most recent applications of DFT, however, adopt segment-level intermolecular forces following either the CMS theory or the generalized thermodynamic perturbation theory.[89] The former is based on a quadratic density expansion of the Helmholtz energy functional with respect to that for a system of ideal chains, much like the methods used for simple or charged fluids.[90-92] This approach requires as input the direct correlation functions from the polymer integral-equation theory (that is, PRISM[93]) and the intramolecular correlation functions from a single-chain Monte Carlo simulation. Similar to the hypernetted-chain approximation for simple fluids, CMS theory is unable to describe phase transitions such as liquid–vapor coexistence. The generalized thermodynamic perturbation theory was initially introduced by Kierlik and Rosinburg,[89] who built on earlier work by Woodward.[94,95] In this approach, the Helmholtz energy functional includes an exact formalism for the ideal chains that retains the details of bond connectivity and an excess part accounting for the contributions from all nonbonded inter- and intramolecular interactions. The excess Helmholtz energy functional is expressed in terms of a weighted-density approximation for short-range forces and a first-order perturbation theory for chain correlations.[61,96,97] For systems containing only homopolymers, the contribution of chain connectivity to the excess Helmholtz energy functional is

$$F_{ch}^{ex} = k_BT\sum_i\int d\mathbf{r}(1-m_i)n_{0,i}(\mathbf{r})\zeta_i\ln y_{ii}[n_\alpha(\mathbf{r})] \quad (15)$$

where y_{ii} stands for the contact value of the local cavity correlation function[‡] of a uniform atomic fluid and n_α represents the weighted densities as used in Eq. 11. Equation 15 can be readily generalized for applications to block and hetero copolymers.[98-100] In comparison with more traditional approaches for representing the structures and thermodynamic properties of polymeric systems, including the polymer integral

[‡] A cavity correlation function is defined as $y(r) \equiv g(r)\exp[\beta u(r)]$.

equation theory and polymer self-consistent field theory, the polymer DFT has the advantage of versatility for polymeric systems with complex intermolecular interactions.

Research over the past three decades has generated numerous versions of DFT but it is fair to say that at this stage, none of them is universally applicable to arbitrary molecular systems. The wide diversity of different versions of classical DFT reflects not only the variety and complexity of natural phenomena induced by rich molecular architecture and nonbonded interactions, but also the generality of the basic idea of DFT and its applicability to a broad range of problems. For practical applications, the selection of a particular version of DFT is influenced by several factors, including not only by its numerical performance in terms of both accuracy and computing efficiency, but also by the underlying physical models, by the problems of interest and, very often, by personal taste. The approximate expressions for the excess Helmholtz energy functional discussed here allow us to address quantitatively most nonbonded interactions in a complex fluid. However, significant efforts are still required for the development of more accurate density functionals accounting for more realistic intermolecular forces. Although the mathematical framework of DFT is exact, its successful application critically depends on judicious choice of an appropriate Helmholtz energy functional suitable for the system under investigation.

Surface Tension and Interfacial Properties

Interfacial properties of fluids are essential for industrial operations involving thin liquid films, emulsions, foams, dispersions, adsorption-based separations, and heterogeneous chemical reactions.[101-104] Traditional phenomenological methods for modeling interfacial properties provide little insight into the microscopic properties of an interface that exhibits inhomogeneity within only a few molecular layers. Detection of the microscopic structure at such a small-length scale defies even the most powerful experimental tools presently available. As a result, much recent progress toward understanding interfacial phenomena relies on molecular modeling.

As discussed earlier, the usefulness of DFT for modeling interfacial properties has been long recognized. Once an interfacial density profile is derived from minimization of the grand potential, the surface energy or interfacial tension can be calculated from

$$\gamma = \frac{1}{A}\left[\Delta\Omega + \sum_i \int d\mathbf{r}\mathbf{r}\cdot\nabla\psi(\mathbf{r})\rho_i(\mathbf{r})\right] \qquad (16)$$

where A stands for surface area, $\Delta\Omega = \Omega - \Omega_b$ is the deviation of the grand potential from that corresponding to the bulk fluid, and $\psi_i(\mathbf{r})$ is the external potential. Equation 16 can be used for an interface between two coexisting phases (such as vapor–liquid and liquid–liquid interfaces) as well as for that between a fluid and a solid substrate. In the former case, there is no external potential and in the latter case the external potential corresponds to the interaction between a molecule and the substrate. Although the interfacial tension calculated from Eq. 16 can be directly tested with experimental data, the density profiles derived from DFT provide insights into the microscopic structure of the interface not available from experiments.

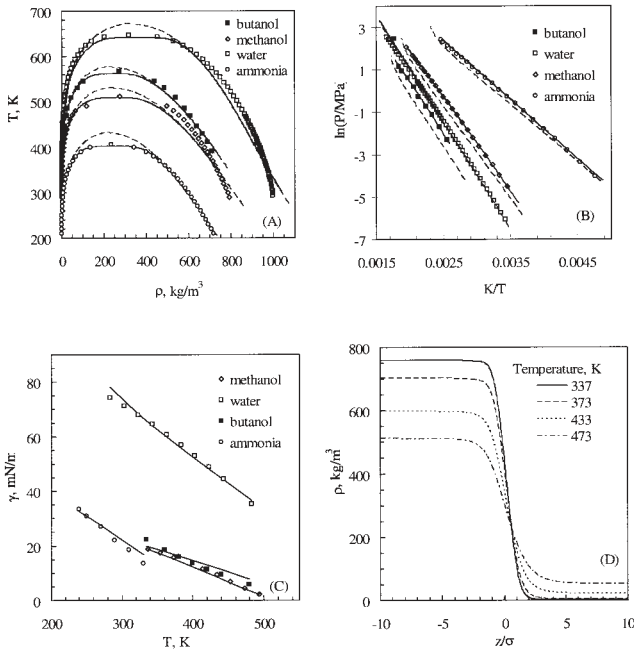

Figure 3. Vapor–liquid coexistence curves (A), saturation pressures (B), and surface tensions (C) for four common fluids from experiment (symbols) and from DFT (lines).[105]

In (A) and (B), the dashed lines show theoretical results without corrections from the renormalization-group (RG) theory for the long-range correlations near the critical point. (D) shows the density profiles at the vapor–liquid interface of methanol.

Because DFT is applicable to both bulk and interfacial systems, it offers a self-consistent approach to describe bulk and interfacial properties using a single molecular framework. Such self-consistency is highly valuable at least from a practical perspective because, although bulk properties, including the phase diagram, are often readily accessible by simple experiment, measurement of interfacial properties is often a much more difficult task.

Vapor–liquid interface

With proper boundary conditions for the coexisting bulk phases, even relatively simple expressions for the Helmholtz energy functional, including van der Waals' original work or those based on the local density approximations (LDAs) or mean-field approximations, are often sufficient to describe semiquantitatively the vapor–liquid interfacial tensions. However, a more sophisticated version of DFT is required to represent the bulk and interfacial properties within a self-consistent theoretical framework. To illustrate, Figure 3 presents the vapor–liquid coexistence curves, vapor pressures, surface tensions, and interfacial density profiles of four common solvents calculated from DFT.[105] In these calculations, the Helmholtz energy functional contains an ideal-gas term, the modified fundamental measure theory for short-range repulsion, a quadratic approximation for van der Waals attractions (Eq. 12), and the thermodynamic perturbation theory for association and chain correlation. The good agreement between theory and experiments near the critical point of the bulk phase diagram is

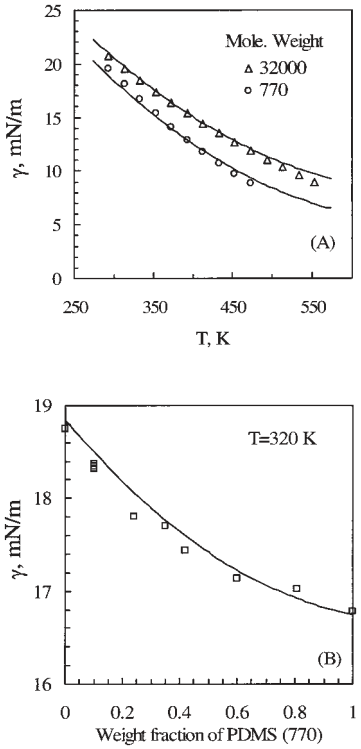

Figure 4. Surface tension of polydimethylsiloxane (PDMS) from DFT (lines) and from experiment (symbols).

(A) The effect of temperature on surface tension for two monodisperse fractions of PDMS with molecular weights 32,000 and 770 Daltons, respectively. (B) The surface tension of a PDMS blend vs. the weight fraction of the low molecular weight polymer. The experimental data are from Dee and Sauer[113] and the lines are calculated by Kierlik et al.[107]

achieved by application of the renormalization group theory.[106] Despite some discrepancy between theory and experiment for the densities of liquid water and methanol resulting from the simplicity of the molecular model, DFT is able to correlate the bulk and interfacial properties at all temperatures in a self-consistent manner. The theoretical description of surface properties is much more demanding than that for bulk properties because it is necessary to consider the spatial inhomogeneity. For this reason, conventional phenomenological models often require additional interface-specific parameters.

A similar DFT can be used to predict the vapor–liquid interfacial properties of polymeric,[107,108] ionic,[109-111] and surfactant systems.[112] For example, Figure 4 shows the temperature dependency of the surface tension of polydimethylsiloxane (PDMS) calculated from a generalized first-order perturbation theory.[107] Agreement of the theory with experiment is excellent for both monodisperse polymers as well as for blends over a wide range of temperature. Although similar performance might be achieved based on a conventional phenomenological theory such as the square-gradient theory,[113] in contrast to DFT, a phenomenological model requires an analytic equation of state for bulk fluids and a few parameters to account for interfacial inhomogeneity. Moreover, the square-gradient theory is unable to capture the nonmonotonic density profiles across the vapor–liquid interface near the triple point or the surface segregation effects arising from branching, segment size, and isotopic substitutions.

As observed in experiments, DFT predicts that, at a given temperature, the vapor–liquid surface tension of a polymeric fluid declines with the chain length or the polymer molecular weight (Figure 5). Numerical results from DFT also suggest that at the vapor–liquid interface of a mixture containing deuterated and protonated polymers of the same length, the deuterated component always partitions preferentially to the interface, but when the protonated chains are much shorter than those of the deuterated chains, the protonated chains are enriched at the interface. These predictions are in good agreement with neutron reflectivity and second-ion mass spectrometry experiments.[107] In addition, DFT captures the accumulation of branched chains at the vapor–liquid surface in a mixture of linear and branched polymers with the same number of repeating units. For the effect of segment-size disparity on surface segregation, DFT correctly predicts a strong surface enhancement of the chains with the larger segment. The predictions of DFT for the vapor–liquid interfacial tensions of ionic fluids and ionic melts are also in good agreement with simulation and experimental results.[110]

Liquid–liquid interface

Demixing of a liquid mixture may occur at both high and low temperatures. For a binary liquid mixture consisting of nonpolar molecules of similar size, demixing occurs only below an upper critical solution temperature (UCST). However, the situation is much more complicated if the molecules of two

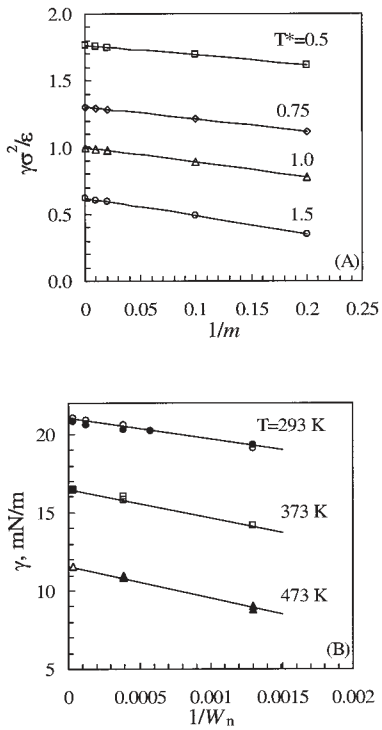

Figure 5. (A) Reduced surface tension vs. the degree of polymerization predicted by DFT;[107] (B) surface tension of PDMS vs. number-averaged molecular weight W_n.

In (A) m is the number of repeating units in each molecule represented by a tangent chain of Lennard–Jones (LJ) spheres, σ and ε are the LJ parameters, and $T^* = k_B T/\varepsilon$.

liquids exhibit large size disparity (such as polymer solutions) or form hydrogen bonds. In that case, the mixture may become immiscible at both low and high temperatures, giving either closed-loop–type or hourglass-type phase diagrams.

DFT has been used to examine the liquid–liquid interfacial behavior of nonpolar,[114] hydrogen-bonding,[115,116] and polymer liquid mixtures.[108,117] In general, a weighted-density approximation is required to reproduce the oscillatory density profiles and a minimum overall density across a liquid–liquid interface. For liquids exhibiting closed-loop immiscibility, it has been shown that the interfacial tension exhibits a maximum at the temperature corresponding to the widest immiscibility gap or equivalently, when the compositions of the coexisting liquids have minimum similarity.[115] The immiscibility loop diminishes either by increasing the association between different components or by reducing the overall density. DFT also predicts demixing of two polymers induced by a difference in chain length and segment diameter.[108,118] The size-induced demixing phase transition is most likely to occur at high pressures. Upon approaching the critical point, the numerical results from DFT indicate that the interfacial tension vanishes as the cube of the density difference between the coexisting phases (as implied by a typical mean-field argument).

For a polymer in a good solvent, the effective interaction between the centers of mass of two polymer chains can be approximately represented by a spherically symmetric Gaussian model.[119] Within this drastically simplified framework, it has been shown that, by using a mean-field expression of the Helmholtz energy functional (random-phase approximation), the density profiles across the coexisting homopolymer/star-polymer mixtures may exhibit pronounced oscillations on both sides of the interface.[120] It was also demonstrated that the crossover from monotonic to damped oscillatory decay in the free interface density profile is determined by the Fisher–Widom line, that is, the line in the bulk phase diagram at which the asymptotic decay of the radial distribution functions crosses over from monotonic to damped oscillatory.[121]

Isotropic–nematic interface

The structure of a planar interface between coexisting nematic and isotropic phases of a liquid crystal is distinguished from that between two isotropic fluids as a result of the existence of long-range orientational ordering. In this case, the surface energy or interfacial tension may vary with the direction of molecular ordering. Onsager's theory represents a simple version of DFT for anisotropic fluids and liquid crystals. At the nematic–isotropic interface, the normal pressure is constant and equal to $-\Omega/V$ (negative of the grand potential density) in both bulk phases at coexistence. However, the transverse pressure P_T is anisotropic and varies with the interfacial density profile. According to Onsager's theory, P_T is given by

$$P_T(z)/k_BT = \rho(z) - \frac{1}{2}\int d\mathbf{r}_{12}\int d\omega_1\int d\omega_2 f(\mathbf{r}_{12},\omega_1,\omega_2) \times \int_0^1 d\lambda\,\rho(z-\lambda z_{12},\omega_1)\rho[z+(1-\lambda)z_{12},\omega_2] \quad (17)$$

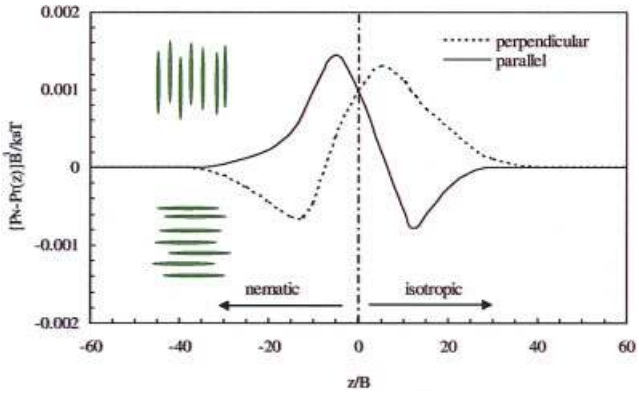

Figure 6. Difference between the normal and transverse pressures across a nematic–isotropic interface (dashed–dotted line) predicted by Onsager's theory.[122]

The liquid-crystal molecules are represented by hard ellipsoids with aspect ratio A/B = 15, where A and B stand for the symmetry axis and the transverse axis of the ellipsoid, respectively. The solid curve applies when the liquid-crystal molecules are aligned parallel to the interface, whereas the dashed line applies when the liquid-crystal molecules are aligned perpendicular to the interface. [Color figure can be viewed in the online issue, which is available at www.interscience.wiley.com.]

where $\mathbf{r}_{12} = \mathbf{r}_1 - \mathbf{r}_2$ is the vector connecting the positions of two molecules at $\mathbf{r}_1$ and $\mathbf{r}_2$, and z is the perpendicular distance from the interface, $z_{12} = z_2 - z_1$, and λ is a coupling parameter.

Figure 6 shows the prediction of Onsager's theory for the difference between normal and transverse pressures in a hard-ellipsoid model of liquid crystals. When the liquid-crystal director in the nematic phase is parallel to the interface, there is a large tension on the nematic side of the interface and a small compressive region on the isotropic side. By contrast, for perpendicular alignment, the tension is on the isotropic side.[122] The variations of the transverse pressure, interface tensions, and density profiles with the liquid-crystal director predicted by Onsager's theory are in good agreement with Monte Carlo simulations.

Effect of surfactants

A conventional approach for interpreting the effect of surfactants on interfacial properties is by measuring the interfacial tension as a function of bulk concentration. The equilibrium adsorption isotherm is then correlated with a phenomenological equation that typically ignores the configuration of surfactant molecules at the interface.[123] By contrast, a theoretical approach based on DFT accounts for both the surface enrichment and configuration of surfactant molecules at the interface.

A new DFT method for describing the effect of surfactants on surface tension and adsorption isotherms has recently been proposed by Stoyanov and coworkers.[124] In this method, the excess surface Helmholtz energy functional consists of a local density approximation for the chain elastic energy of surfactant molecules and the surface osmotic pressure[124]

$$F^{ex} = \int dz[K_s z^2\phi + (1-2\chi)k_BT\phi^2/2v_{solv}] \quad (18)$$

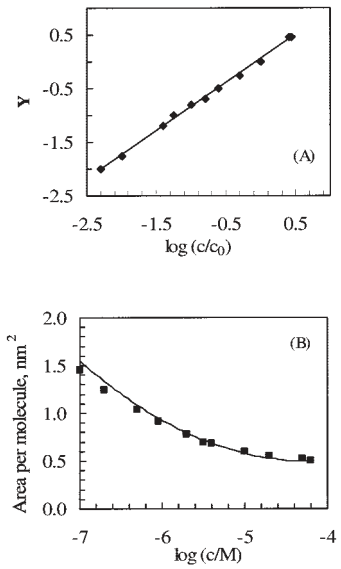

Figure 7. (A) A new scaling relation between the surface pressure (Π) and the bulk concentration of *n*-dodecyl pentaoxyethylene glycol ether (C12E5) at the air–water interface; (B) surface area per C12E5 molecule vs. bulk concentration of the surfactant from SANS/ellipsometry measurements (points) and from DFT (lines) (reproduced from Stoyanov et al.[124]).

In (A) $Y = \Pi^{2/5} - \Pi_0^{2/5}$, where subscript "0" denotes an arbitrary reference point, c stands for molar concentration (M).

where K_s is the elastic constant of the chain molecule, ϕ represents the local volume fraction of the surfactant, χ is the Flory parameter, and v_{solv} is the solvent molecular volume. Based on Eq. 18, Stoyanov et al. showed that the surface pressure, defined as the difference between the interfacial tensions without and with surfactant molecules, $\Pi = \gamma_p - \gamma$, follows the scaling relation[124]

$$\Pi^{2/5} \sim \frac{2k_BT}{5\alpha^{3/5}} \ln c \tag{19}$$

where $\alpha = [(18/25)w^2K_s(mv_0)^5]^{1/3}$ and $w = (1 - 2\chi)k_BT/v_{solv}$; m and v_0 are the number of segments and the segment volume of the surfactant molecule, respectively; and c is the surfactant molar concentration. Figure 7A shows the surface pressure as a function of the bulk surfactant concentration derived from Eq. 19. The agreement of theory with experiment is truly remarkable, bearing in mind the simplicity of the theoretical model. Figure 7B shows the predicted surface area per surfactant molecule as a function of surfactant concentration. The theoretical predictions are again in good agreement with experimental data from small-angle neutron scattering (SANS) and ellipsometry measurements.

Capillary waves

The vapor–liquid and liquid–liquid interfaces are presumed planar in all the above discussions. However, in general, both interfacial density profiles and surface tension depend not only on the intermolecular forces but also on the capillary waves of the interface. Using an effective interface Hamiltonian derived from DFT and a Gaussian approximation for distortion of the planar density profile, Mecke and Dietrich[125] predicted that the surface tension first declines with surface-wave vector q, attains a minimum, and then grows as q^2 for large q. In other words, a negative correction must be applied to the surface tension if the interface shows a large curvature. Because of the reduction in surface tension, the interface deformation becomes more likely at small-length scales. This prediction contradicts results from a conventional capillary-wave model but has been confirmed by experimental results from X-ray surface scattering.[126] In most cases, the capillary wave has a more significant influence on the density profiles than on the surface tension.

Gas Adsorption and Materials Characterization

Gas adsorption is a broad subject relevant to numerous industrial applications ranging from natural gas recovery, fuel storage, and CO_2 sequestration to sensors for chemical warfare agents and to the treatment of lung diseases.[127] As proposed by the IUPAC Commission on Colloid and Surface Chemistry, the equilibrium behavior of gas adsorption at a solid substrate can be classified into six basic types depending on the strength of gas–substrate interactions and on the pore size. Figure 8 schematically shows adsorption isotherms according to the IUPAC classification.[128] Type I is typical for gas adsorption in microporous materials such as activated carbon and zeolites with pore size $\lesssim 2$ nm. Types II and III correspond to adsorption in macroporous or on nonporous materials with strong and weak fluid–surface attractions, respectively. Types IV and V are typical for mesoporous materials (with pore size between 2 and 50 nm) with strong and weak surface attractions; both exhibit a hysteresis loop in adsorption and desorption. Type VI applies to systems with strong surface–gas interactions and when the temperature is near the triple point of the adsorbate.

Classical DFT provides a state-of-the-art technique for modeling gas adsorption at the molecular level. It enables calculations not only of adsorption isotherms but also of the detailed inhomogeneous density profiles of gas molecules and of surface phase transitions.[129,130] Unlike conventional semiempirical theories such as Langmuir, Brunauer–Emmett–Teller (BET), and Kelvin equations, and numerous variations and extensions

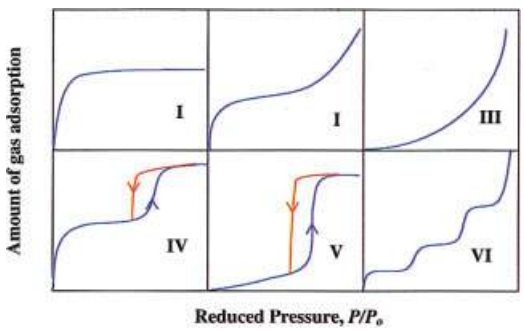

Figure 8. IUPAC classifications of gas adsorption isotherms.

Here P_0 stands for the gas saturation pressure. [Color figure can be viewed in the online issue, which is available at www.interscience.wiley.com.]

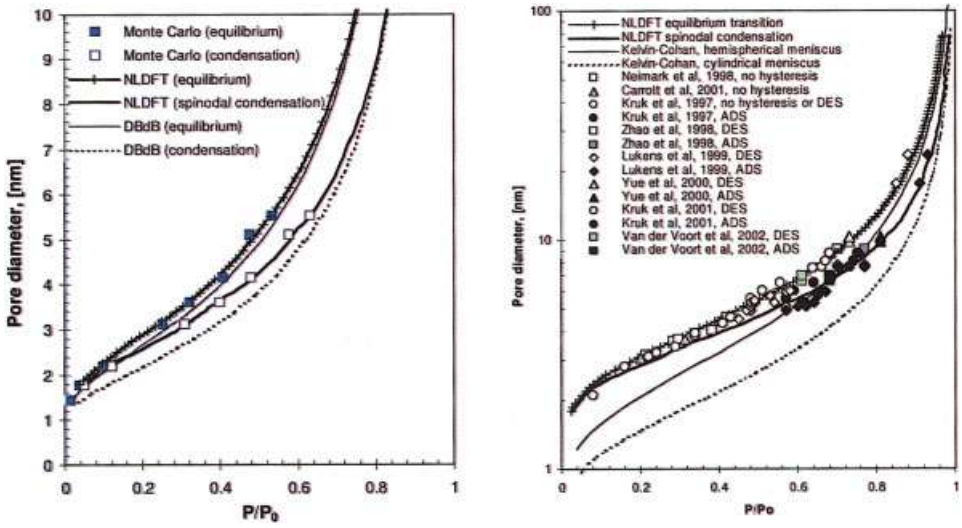

Figure 9. DFT bridges scales from molecular simulations to classical thermodynamics for modeling gas adsorption.

(a) Pressures of capillary condensation and desorption of argon at 87.3 K in a cylindrical pore predicted by NLDFT, by gauge-cell Monte Carlo simulation, and by phenomenological Derjaguin–Broekhoff–de Boer (DBdB) theory. (b) Relative saturation pressures for the adsorption (ADS) and desorption (DES) of N_2 at 77 K in MCM-41 and SBA-15 nanoporous materials predicted by DFT and by the Kelvin–Cohan equation. The points are experimental data.[133] [Color figure can be viewed in the online issue, which is available at www.interscience.wiley.com.]

of these classical methods, DFT is able to describe quantitatively all six types of adsorption isotherm within a unified framework. For example, Balbuena and Gubbins[131] investigated adsorption of an argon-like fluid in a graphite-like slit pore using a nonlocal density functional theory (NLDFT). Their model system consists of Lennard–Jones molecules adsorbed in a single slit pore where the wall potential is specified by Steele's 10-4-3 potential

$$\psi_s(z) = \varepsilon_w\left[\frac{2}{5}\left(\frac{\sigma_w}{z}\right)^{10} - \left(\frac{\sigma_w}{z}\right)^{4} - \frac{\sigma_w^4}{3\Delta(z+0.61\Delta)^3}\right] \quad (20)$$

where the parameters ε_w, σ_w, and Δ are related to the properties of the solid substrate. The excess Helmholtz energy functional includes a hard-sphere term proposed by Tarazona[132] and an attractive term represented by the mean-field approximation

$$F^{ex}[\rho(\mathbf{r})] = F^{ex}_{hs}[\rho(\mathbf{r})] + \frac{1}{2}\int\int d\mathbf{r}_1 d\mathbf{r}_2 u_{att}(\mathbf{r}_1 - \mathbf{r}_2)\rho(\mathbf{r}_1)\rho(\mathbf{r}_2) \quad (21)$$

Balbuena and Gubbins[131] studied the variation of adsorption behavior as a function of surface energy and pore width. They found that NLDFT is able to reproduce all six types of adsorption isotherms according to the IUPAC classification. More recently, Neimark and coworkers[133] also demonstrated that, as reproduced in Figure 9, DFT properly bridges the gap between molecular simulations and phenomenological equations, thereby providing a description of capillary condensation/evaporation at all length scales.

Application of DFT for gas adsorption is not limited to nanostructured materials such as zeolites, MCM-41, or aluminophosphates where the microscopic structure can be determined by X-ray or neutron diffraction.[134] In recent years, DFT has also been used for characterization of amorphous materials such as activated carbons, oxides, or silica gels where we lack definite knowledge of the pore structure.[135]

The mean-field approximation for representing the van der Waals attractions between gas molecules becomes inadequate when the surfaces are weakly attractive. As an improvement, a number of more sophisticated versions of DFT have been proposed in the past few years.[136-138] To illustrate, Figure 10 shows density profiles for a Lennard–Jones fluid near a hard wall and in an attractive slit pore calculated from Monte Carlo simulations and from two different versions of DFT.[54] Although the mean-field theory is excellent for adsorption in the attractive slit pore, its performance near a hard wall is inferior to that of a non-mean-field version that takes appropriate account of correlation effects.

In addition to adsorption and capillary condensation of simple fluids, DFT is useful for describing liquid–liquid demixing under confinement. For simple binary mixtures of nonpolar liquids in a slit-like pore, classical DFT predicts that, in general, the confinement and the wall attraction depress the UCST and the region of immiscibility.[117] If the confining surface preferentially attracts one component in the binary mixture, the confinement leads to a shift of the coexistence curve toward the phase that is rich in the preferred component.[139] Similar calculations have been reported for binary mixtures of associating liquids that exhibit closed-loop immiscibility.[116] For polymer mixtures, a DFT calculation indicates that, when the confining surface is attractive, confinement in slit-like pores leads to a two-step demixing transition.[140] The first step of demixing occurs within a few layers adjacent to the attractive surface and the second step occurs in the entire pore. The multistep demixing transitions of confined Gaussian-core fluids are strikingly similar to the condensation and layer transitions of associating fluids and water in attractive micropores.[141,142] The effects of confinement on liquid–liquid separations revealed by DFT

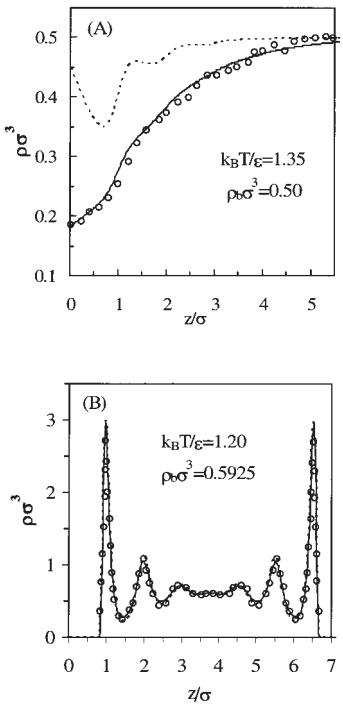

Figure 10. Density profiles of a Lennard–Jones fluid (A) near a hard wall and (B) in an attractive slit pore.

The points are results from Monte Carlo simulation; the solid and dashed lines are predictions of DFT using the direct correlation function and the mean-field approximation, respectively.[54]

provide useful insights for applications in oil recovery, lubrication, coating technology, and pollution control.[139]

Wetting Transitions

Wetting refers to the disappearance of the contact angle of three coexisting phases, such as a liquid droplet setting on a solid substrate surrounded by a saturated vapor phase. The phenomenon is pertinent to the spreading of paint on a wall, spraying of an insecticide on leaves, extrusion of textile fibers from a liquid solution, lubrication of gears, aircraft deicing, and crude oil recovery from porous sandstones. The literature on wetting phenomena is vast; a number of excellent reviews have been published on both experiment and theory.[143,144] Below we review only some salient features of wetting behavior in the context of recent work based on DFT.

A simple fluid near a planar wall

Most theoretical work on wetting phenomena has been focused on a simple model system consisting of a vapor phase (saturated or unsaturated) in direct contact with a smooth planar solid. Because of the surface attraction, a thin layer of a liquid-like film is formed at the solid substrate even when the vapor phase is unsaturated. As shown in Figure 11, at a given temperature the film thickness increases monotonically with the vapor pressure and reaches a finite value below the wetting temperature T_w, but diverges otherwise. Below T_w, a bulk liquid partially wets the surface. In this case, the contact angle is related to the vapor–liquid, vapor–solid, and liquid–solid interfacial tensions according to Young's equation. Above T_w, the saturated liquid completely wets the surface and the contact angle becomes zero. At certain conditions, a thin–thick film transition may occur below the saturation pressure. This phenomenon is known as prewetting. The prewetting transition has its own critical point referred to as the surface critical temperature $T_S{}^C$. Above $T_S{}^C$, there is no coexistence of the thin and thick films. Depending on the strength of the surface-fluid potential, the surface critical temperature can be either below or above the bulk critical point.

In analogy to bulk phase transitions, a wetting transition can be first or second order, depending on whether the film thickness diverges discontinuously or continuously as the temperature increases.[‡‡] In some special cases, the second-order wetting transition may be preceded by a first-order, microscopic-to-mesoscopic film transition known as pseudopartial wetting[145] or frustrated complete wetting.[146] Figure 12 shows three wetting scenarios. The boundary between first-order and second-order wetting transitions is shown in terms of the surface energy when the attraction between the substrate and fluid is short range.

Prewetting transition was first predicted by Ebner and Samm[147] using a gradient expansion of the Helmholtz energy functional and by Cahn[40] using van der Waals' square-gradient theory. The adsorption isotherm shows a discontinuity at the condition of a prewetting transition, where a thin liquid film coexists with a thick liquid film at the same temperature and at a pressure below the saturation. The density profiles of both the thin and thick films satisfy the variational equation (Eq. 4) and they yield the same grand potential. Similar prewetting transitions were discovered later in the binary liquid mixture methanol and cyclohexane in contact with the coexisting vapor phase.[148] Because of the drastic approximations used in the early theories, the existence of the first-order prewetting transition resulted in controversy that stimulated a number of

[‡‡] At the wetting transition, the liquid always coexists with a saturated vapor. By contrast, prewetting occurs at a pressure below the saturation.

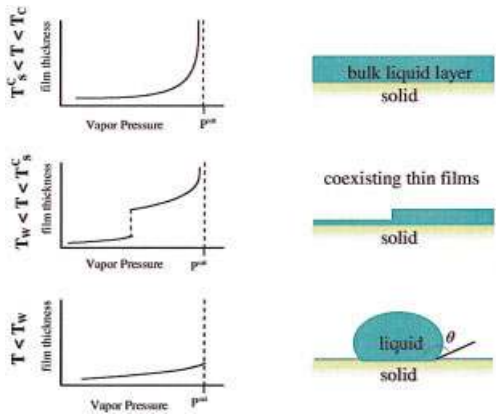

Figure 11. Film thickness vs. vapor pressure at different temperatures.

Here T_w = wetting temperature, T_C = bulk critical temperature, and $T_S{}^C$ = surface critical temperature. [Color figure can be viewed in the online issue, which is available at www.interscience.wiley.com.]

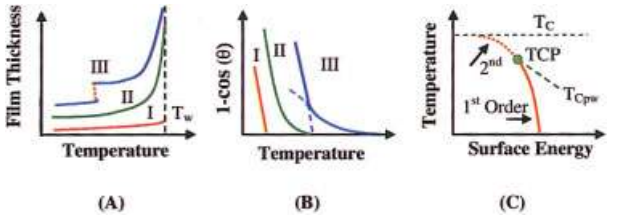

Figure 12. (A) For a solid in contact with a saturated vapor (that is, *at vapor–liquid coexistence*), a thin liquid film is formed at the solid surface and its thickness diverges smoothly or discontinuously as the temperature approaches the wetting point (T_w): (B) variation of the contact angle θ near the wetting temperature: (I, II, and III stand for first-order, second-order, and sequence of wetting transitions, respectively); (C) when the fluid–solid interaction is short range, the first-order and the second-order wetting-transition lines join at the tricritical point (TCP) where the prewetting critical temperature (T_{Cpw}) terminates.

[Color figure can be viewed in the online issue, which is available at www.interscience.wiley.com.]

simulation works.[22] Quantitative agreement between DFT and Monte Carlo simulations can be seen in recent theoretical investigations of prewetting transitions.[149]

Cahn's theory has been extended to ionic fluids[150] and to systems with long-range substrate–fluid interactions where frustrated complete wetting may occur.[151] Nakanishi and Fisher[152] demonstrated that it is able to capture most features of prewetting and wetting transitions if the surface attraction is short range. Regrettably, Cahn's theory is mostly qualitative; it provides only an appropriate connection between surface behavior and molecular properties of the solid and the coexisting fluid. With the advent of more sophisticated versions of classical DFT, the coarse-grained theory has gradually fallen out of fashion. DFT is useful especially for investigating wetting transitions of complex fluids including polymeric systems. In addition to first-order and second-order wetting transitions and prewetting, DFT is able to capture the dependency of wetting behavior on the details of substrate–fluid interactions and the sequential wetting behavior at some subtle conditions of the

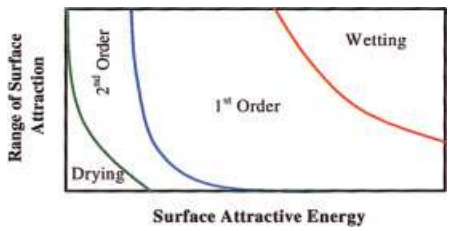

Figure 13. Effect of surface-fluid potential on wetting transitions predicted by DFT.[156]

In the drying zone, the contact angle is always nonzero, whereas in the wetting zone, the liquid completely wets the surface at all temperatures. Between the drying and wetting zones, the wetting transition can be either first or second order. [Color figure can be viewed in the online issue, which is available at www.interscience.wiley.com.]

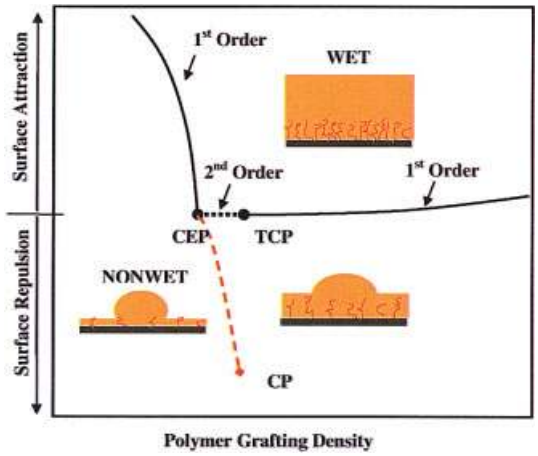

Figure 14. Wetting behavior of a polymer on a polymer-tethered surface predicted by DFT.[280]

The solid lines denote first-order wetting transitions; the horizontal line marks second-order wetting transitions; and the broken curve denotes transitions between a microscopic thin film and a mesoscopic thick film. The line giving transitions between a thin and a thick film terminates at a critical end point (CEP) and at a critical point (CP). The second-order and first-order wetting transitions at high grafting densities are separated by a tricritical point (TCP). [Color figure can be viewed in the online issue, which is available at www.interscience.wiley.com.]

long-range solid–fluid interactions.[153-155] Figure 13 schematically shows a phase diagram of wetting transitions in terms of the surface energy according to a simple mean-field approximation of the Helmholtz energy functional for a nonpolar fluid in contact with an attractive solid.[156,157] As observed in experiments, second-order wetting is most likely when the fluid–surface interaction is short range and only moderately attractive. In addition, DFT predicts complete wetting and nonwetting zones at strongly and weakly attractive surfaces, respectively.

Wetting of polymeric fluids

Qualitatively, the wetting behavior of a polymeric fluid resembles that for atomic systems.[158,159] Essentially the same theories (such as Cahn's theory or classical DFT) can be used to describe prewetting and various forms of wetting transitions in polymeric systems.[144,160,161] For example, DFT has been applied to predicting the wetting behavior of a polymer melt on a surface tethered with polymer chains of the same kind.[144] This system is relevant to dielectric coating, adhesion, lubrication, and biocompatibility. As shown in Figure 14, the polymer DFT predicts a first-order wetting of the polymer melt at an attractive surface with low grafting densities, similar to that on a bare surface. For neutral or weakly attractive surfaces, however, the wetting transition is second order at intermediate grafting densities and becomes first order again at high surface grafting densities. The theory predicts a frustrated complete wetting on a repulsive surface resembling that for a simple fluid reported recently.[162] These predictions have subsequently been observed in experiments.[163,164] In addition, Muller and MacDowell studied the influence of an oxide layer on the wetting behavior of polystyrene on top of a silicon surface. This system represents a frequently used experimental situation for studying

wetting and dewetting phenomena in polymeric systems. At the silicon surface with a thin oxide coating layer, DFT predicts that the surface free energy is everywhere positive relative to that of the bare surface or when the surface is in direct contact with the bulk liquid. In this case, the polymer partially wets the surface. When the surface is coated with a thick layer of oxide, on the other hand, a polymer film of finite thickness is stable, corresponding to the state of frustrated complete wetting. Below the frustrated complete wetting temperature, the mesoscopic film ruptures into small droplets. Prediction of "nanodewetting" is in good agreement with experiment.[165]

Effect of curvature on wetting

DFT has also been applied to investigating the influence of substrate curvature on wetting transitions.[166-168] Unlike the planar case, complete wetting does not occur on a spherical particle where the thickness of the wetting layer grows only as the logarithm of the particle radius.[169] DFT predicts that at a spherical substrate, the contact angle declines with curvature, whereas the opposite holds for the wetting temperature.[170]

Solvation and Surface Forces

In the development of modern solution theories, one key challenge is to understand the microscopic structure of solvent molecules near a solute (that is, solvation) and the solvent-mediated forces. There has been a vast literature concerning solvation and solvation forces. The following discussion is limited to a few cases relevant to recent applications of DFT to colloidal systems.

Solvation at different length scales

The presence of a solute in a liquid solvent introduces a local distribution of solvent molecules that is affected not only by solute–solvent interactions but also by the size of the solute. Although the effect of the solute–solvent interaction energy on solvation is well documented, the size effect is much more subtle, as first indicated by Stillinger more than 30 years ago.[171] By separately considering the slow and fast-varying components of the local inhomogeneity using respectively the van der Waals' square-gradient theory and Gaussian approximation (or quadratic density expansion), Lum et al.[172] demonstrated that the solvation of small apolar groups in water is different from that of large hydrophobic groups. In the former, hydrogen bonding of water is hindered yet persists near the solute. In the latter, hydrogen bonding is depleted, leading to drying of extended apolar surfaces and to long-range hydrophobic attraction.

Accumulation of solvent molecules near a small solute, and depletion of solvent molecules near a larger solute has also been observed in simple fluids as represented by the hard-sphere or Lennard–Jones (LJ) potential.[54,173] Figure 15 shows the distributions of LJ molecules in a stable liquid around an isolated hard-sphere solute of different sizes.[174] Even in the absence of solute–solvent attractions, solvent molecules may accumulate around a solute whose size is comparable to that of the solvent. The oscillatory local density distribution resembles the radial distribution function of the pure solvent (Figure 15). In this case, the solvation force is short range and mainly repulsive. With increasing solute size, however, the oscillatory

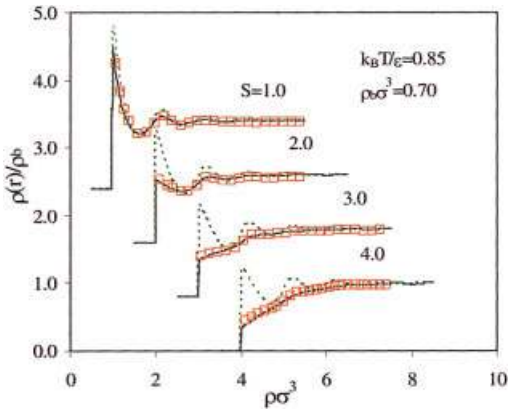

Figure 15. Density profiles $\rho(r)$ of a Lennard–Jones (LJ) fluid around an isolated hard sphere of different sizes.[54]

Here ρ_b is the bulk density of the LJ fluid and S stands for the size ratio, that is, the diameter of the hard sphere divided by σ. The symbols are simulation data,[281] and the solid and dashed lines are predictions of DFT. For clarity, the density profiles for $S = 1$, 2, and 3 have been shifted upward by 2.4, 1.6, and 0.8 units, respectively. [Color figure can be viewed in the online issue, which is available at www.interscience.wiley.com.]

density profile rapidly fades away and a vapor-like layer is developed near the solute surface. The thickness of the vapor-like layer grows with solute size, leading to a long-range attraction.[175,176]

With an appropriate formulation of the excess Helmholtz energy functional, agreement between DFT and molecular simulation is nearly perfect.[174] Results from DFT calculations also suggest that the depletion-induced surface attraction is substantially stronger than that expected from conventional Hamaker or Lifshitz theories.[175] In addition, DFT predicts that, in good agreement with molecular simulations but contrary to the standard Hamaker theory, in a fluid medium the attraction between two hard surfaces increases with temperature when the pressure is fixed, but at a fixed temperature, it falls as the pressure rises.[175] Because the van der Waals attraction between solute and solvent molecules is ubiquitous, even a weak solute–solvent attraction may lead to a large reduction of the vapor-like depletion layer. Nevertheless, the incipient presence of drying should play an important role in hydrophobic phenomena at large-length scales.[172,177]

Electric double layer

The solvation of a charged particle in an electrolyte solution results in the accumulation of counterions and the depletion of co-ions. The charged surface, along with the neutralizing counterions, is called the electric double layer (EDL), which is of central importance in surface chemistry and colloid science. Although conventional wisdom suggests that the colloidal charges are only partially screened by the surrounding counterions, recent experiments and molecular simulations indicate that the overall charge of a macro-ion plus that of its surrounding counterions may have a sign opposite to its bare charge.[178,179] In contradiction to classical Derjaguin–Landau–Verwey–Overbeek (DLVO) theory, the electrostatic interaction between similarly charged colloidal particles can be attractive

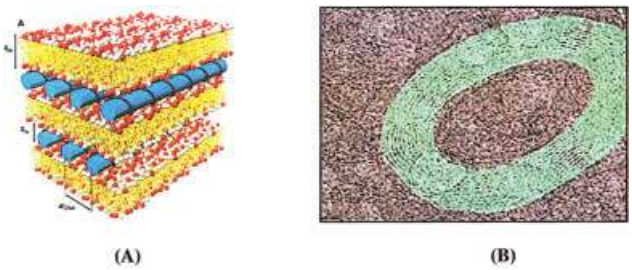

Figure 16. Understanding nonintuitive electrostatic phenomena such as charge inversion and attraction between similar charges could lead to more efficient strategies for gene therapy.

(A) Lipid–DNA complex where the lipid molecules are arranged in a lamellar stack of nearly flat bilayers, with the DNA intercalated between each pair of bilayers.[183] The DNA molecules are represented by rods with the black lines denoting a helical structure; the light and dark spheres represent the head groups of the neutral and cationic lipid molecules, respectively; and the hydrophobic layer consists of lipid tails. (B) A micrograph of a λDNA toroid.[282] [Color figure can be viewed in the online issue, which is available at www.interscience.wiley.com.]

in the presence of multivalent counterions.[180] These nonintuitive electrostatic phenomena arise from the correlation of small-ion distributions and from the size effect that are neglected in classical electrostatic theories.

Electrostatic interactions are important for a number of technological applications including fabrication of composite materials,[181] intelligent sensors,[182] and gene delivery.[183] Figure 16 illustrates two complex structures formed by charge inversion and subsequent attraction between similar charges. Each lipid bilayer adsorbs an excess amount of oppositely charged DNA molecules leading to the charge inversion, which allows the assembly of additional lipid layers. In other words, two lipid layers of the same charge exhibit strong attraction (as shown in the well-organized layer-by-layer structure) in the presence of oppositely charged DNA molecules. The attraction between similar charges is also evident from the formation of DNA toroid in the presence of multivalent counterions. Because the DLVO theory ignores the molecular characteristics of small ions, it is apparently insufficient to explain DNA condensation or the formation of DNA–lipid complexes. A good understanding of these mesoscopic structures would be helpful for controlling the structure of assemblies of biomacromolecules for medical applications including more efficient machinery for gene delivery.

Charge inversion and attraction between similar charges can be captured using relatively simple models of colloids where both colloidal particles and salt ions are represented by spherical charged particles and the solvent is a continuum dielectric medium. Even though this primitive model is much oversimplified, it retains the essential physics of the nonintuitive electrostatic phenomena that cannot be described by conventional mean-field theories including the Poisson-Boltzmann (PB) equation. A simplified model may provide useful insights into often complicated realistic systems. By explicitly accounting for the size effect and for the correlation of charge distributions that are ignored by the PB equation, DFT is able to represent both charge inversion and attraction between like charges.[81,184] To illustrate, Figure 17 shows that, at sufficiently high surface-charge density, the overall charge of a macro ion and its surrounding counterions near the surface may become opposite to the bare charge of the macroion. Results from DFT also reveal that, in contrast to the predictions from the PB equation, the zeta potential of a colloidal particle strongly depends on the valence of counterions and may not vary monotonically with the charge density. Recently, DFT has also been applied to investigating the structural and thermodynamic properties of multicomponent mixtures mimicking a crowded cellular environment.[74] In the context of a primitive model where macromolecules are represented by neutral or charged particles and water by a continuous medium, it has been demonstrated that DFT is able to quantitatively account for both the excluded-volume effects and the long-range electrostatic interactions.

Polymer-mediated solvation forces

Dispersions of colloidal particles in polymeric systems have been the focus of sustained experimental and theoretical efforts stemming from their close relevance to colloidal stability and composite materials. However, comprehensive understanding of solvation and interactions between colloidal particles in polymeric systems remains a theoretical challenge. Even at the molecular level, such systems involve multiple length scales arising from the solvent molecules, the polymer segments, the entire polymer chain, and the colloidal particles. Subtle interplay of the particle size, the polymer chain length, the particle–segment interactions, the polymer concentration, and the solution conditions makes the distribution of polymer chains around each particle extremely intricate, thereby leading to delicate colloidal forces and phase behavior. In particular, near the critical point of the solvent phase transition or near the thin–thick film transition at the surface of each colloidal particle, extremely attractive and long-range colloidal forces have been identified.[185-187]

Classical DFT offers a generic approach for quantitative description of solvation and colloidal forces in polymer solutions and melts. In comparison to a number of conventional theories, DFT has the advantage of taking into account the multiple length scales associated with the polymer–colloid systems within a theoretically consistent framework.[188,189] DFT

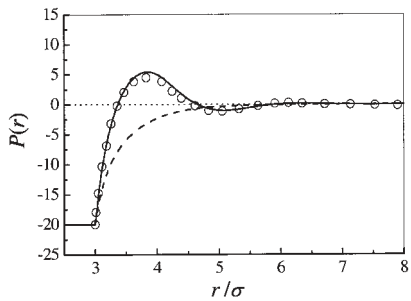

Figure 17. Accumulated charge *P*(*r*) around an isolated macroion in a 2:2 electrolyte solution at *T* = 300 K.[81]

The concentration of the electrolyte is 1.25 M and the diameter of small ions $\sigma = 0.4$ nm. The macroion has radius 1.0 nm and total charge -20. r is the distance from the center of the macroion. The symbols are MC data; the dashed and solid curves represent results from the Poisson–Boltzmann theory and DFT, respectively.[81]

is applicable to dilute and semidilute polymer solutions as well as to polymer melts, polymers of essentially arbitrary architecture, and adsorbing or nonadsorbing polymers.[190]

The distribution of polymers near a colloidal particle and polymer-mediated colloidal forces are significantly influenced by the particle–polymer interaction energy and by the size ratio.[191] In the absence of strong particle–polymer attraction, polymers in a good solvent are depleted from the surface of a large particle on the length scale comparable to the polymer radius of gyration. In this case, the colloidal force is predominantly attractive, as predicted qualitatively by the Asakura–Oosawa theory. The entropy-induced attractive potential increases with polymer concentration. When the polymer concentration is beyond a certain limit, however, the self-exclusion of polymer segments diminishes the depletion zone near the colloidal surface. Competition of surface depletion with excluded-volume effects induces a repulsive barrier in the solvation potential before the colloidal particles fall into deep attraction near contact.[192] Such repulsion could lead to restabilization of a polymer-flocculated colloidal dispersion that cannot be captured by Asakura–Oosawa theory.[96]

Upon addition of strong attraction between colloidal particles and polymer segments, the depletion layer disappears and accumulation of polymer chains near the particle surface leads to a colloidal repulsion. By contrast, more attraction between polymer segments upon changing solvent quality or temperature leads to stronger surface depletion and consequent colloidal aggregation. When the colloidal particle is significantly smaller than the polymer radius of gyration, the distribution of polymer segments near the particle surface is determined by the segment–particle interactions and by the polymer intramolecular correlations. For polymers in a good solvent, recent neutron-scattering experiments suggest that the excluded-volume effects between the polymer segments and the colloidal particles may cause the polymer chains to shrink or collapse significantly.[193] As revealed by Monte Carlo simulations,[194,195] the reduction of polymer size can be explained by polymer wrapping around the colloidal particle. In this case, the potential of mean force between colloidal particles is also attractive. However, this attraction is not introduced by the depletion of polymer chains but probably arises from the excluded-volume effect of polymer segments and the intrachain correlations. The cause of attraction is reflected in the range of colloidal forces that are normally much smaller than the polymer size. At a low polymer concentration, the polymer-mediated potential is very weak ($<0.05k_BT$) but is relatively long-range. Beyond the polymer overlap concentration, the segment-excluded volume becomes more significant and the short-range attraction is considerably enhanced.[196] For small colloids dissolved in a solution of nonadsorbing polymers, recent Monte Carlo simulation also indicates the colloidal force may exhibit long-range oscillation persisting over several multiples of the polymer radius of gyration.[197] Although a full capture of all the details of polymer-mediated colloidal forces represents a significant theoretical challenge, application of DFT to polymer–colloid mixtures is certainly very promising.

It has been long recognized that attachment of highly soluble polymers onto a colloid/solid surface offers an efficient means to minimize often undesirable, nonspecific surface adsorption in a solution and to stabilize colloidal particles.[198,199] The equilibrium properties and surface forces of tethered polymers

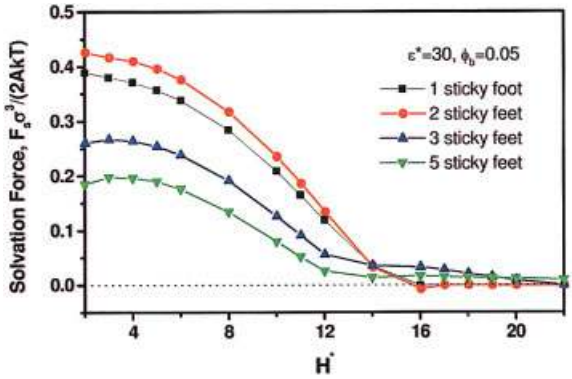

Figure 18. Surface force F_s between two parallel plates mediated by copolymers with multiple anchoring sites.[100]

Here σ stands for segment size, $H^* = H/\sigma$ is the reduced surface separation, $\varepsilon^* = \varepsilon/k_BT$ is the reduced surface energy, A is the surface area, and ϕ_b is the bulk volume fraction of the polymer. The copolymer consists of blocks of 20 nonsticky segments for each surface anchoring site. [Color figure can be viewed in the online issue, which is available at www.interscience.wiley.com.]

(brushes) have been subjected to extensive investigations by experiments, simulations, and a number of theories, including DFT.[200-203] Recent interest has been shifted to studying the effect of polymer architecture, especially branched, star, or multiblock copolymers on surface protection.[190] For example, at fixed surface grafting density, highly branched hydrophilic copolymers minimize protein adsorption more efficiently than traditional linear polymers such as polyethylene glycol.[204] As shown in Figure 18, polymers with multiple anchoring sites may introduce a cooperative effect in terms of both grafting efficiency and solvation forces.[100] Applications of DFT to more complicated polymeric systems will help to narrow the gap between fundamental research and practical applications of soft matter.

Freezing and Melting Transitions

Classical DFT has been widely recognized as one of the most efficient methods for theoretical study of freezing and melting transitions in simple fluids as well as in colloidal dispersions. Despite indisputable success, early application of DFT in this field was for a while regarded as "utilitarian or a chemical engineer's prescription."[22] The main reason is a lack of theoretical justifications for various early versions of weighted density approximations (WDAs) that map the free-energy functional of an anisotropic solid to that of a homogenous fluid. The situation is quite different after the invention of the fundamental measure theory, which has a firm theoretical basis and is naturally applicable to fluids as well as to solids.[205] Different from conventional equations of state that entail different models for coexisting phases, DFT directly expresses the thermodynamic potentials of a system, fluid or solid only, in terms only of one-body density profiles. DFT is able to describe freezing and melting transitions within a unified theoretical framework.

In DFT calculations, the anisotropic solid density is usually specified a priori as a sum of the Gaussian distributions centered on the Bravais lattice sites of the solid phase

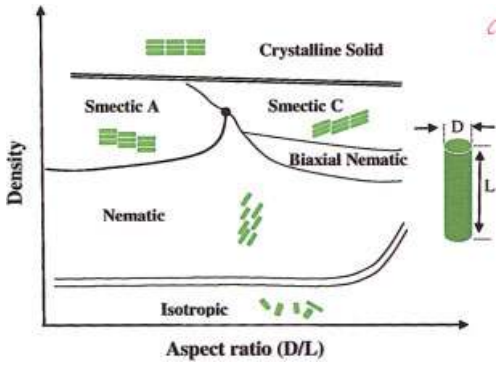

Figure 19. Phase diagram for a system containing hard cylinders according to DFT.[240]

Cylinder shown on the righthand side defines the diameter D and length L of a liquid-crystal molecule. Inserts show alignment of liquid-crystal molecules. [Color figure can be viewed in the online issue, which is available at www.interscience.wiley.com.]

$$\rho(\mathbf{r}) = \left(\frac{\pi}{\alpha}\right)^{3/2} \sum_{\mathbf{L}_i} \exp(-\alpha|\mathbf{r} - \mathbf{L}_i|^2) \tag{22}$$

where the inverse width of the Gaussian parameter α provides a measure of the density localization in the crystal and $\{\mathbf{L}_i\}$ represnts the real-space lattice vectors. With different methods for the paramerization of the solid density, DFT has been successfully applied to representing fluid–solid and solid–solid transitions in hard spheres,[206-209] simple liquids,[210,211] anisotropic fluids,[212-214] and various models of colloidal dispersions.[215-221] DFT is useful not only for freezing/melting transitions of one-component systems but also for mixtures where exotic fluid–solid and solid–solid transitions have been identified.[222-224] Application of DFT to a fluid–solid interface (with explicit consideration of solid inhomogeneity) is able to capture the partially periodic microscopic structure and the orientation variation of the interfacial tension.[225,226] More recently, DFT has been used to explore structure formation in colloids under an external field.[227-229] The periodic potential-induced freezing and reentrant melting of colloidal particles at a surface predicted by DFT are all in good agreement with experiment.[230,231]

Phase Behavior of Liquid Crystals

Liquid crystals are characterized by orientational anisotropy on a macroscopic scale arising from partial ordering of nonspherical molecules. The equilibrium density profile in a liquid crystal depends on both the distribution of the center of mass and the orientation of constituent molecules. The system is in an isotropic state if the density is independent of both position and orientation. As shown in Figure 19, a nematic state is obtained if the density depends on orientation but not on position; a smectic state is obtained if the density is ordered in both position and orientation. Other liquid-crystal states are also possible in confined systems or in those consisting of more complicated liquid-crystal molecules.

Lyotropic liquid crystals

Because the thermodynamic functions of a liquid crystal phase can be naturally expressed in terms of the angle-dependent density profiles, the usefulness of DFT for predicting the phase behavior of liquid crystals has long been recognized. As discussed earlier, Onsager's theory for the isotropic–nematic phase transition in hard rods is based on the second-virial expansion of the excess Helmholtz energy functional.[38,232,233] It is exact for infinitely long hard rods but becomes inadequate for systems containing molecules with a small aspect ratio and for those phase transitions that include various smectic phases. The Parson–Lee functional provides an improvement of Onsager's theory by taking into account the excluded-volume effect using an effective hard-sphere model.[233-236] Likewise, the Maier–Saupe theory and its extensions to include intermolecular attractions can be understood as an extension of van der Waals mean-field theory for uniform fluids to systems with orientation-dependent intermolecular attractions.[237]

Classical theories of liquid crystals are useful for describing isotropic-to-nematic transitions but are often insufficient to represent those phase transitions that concern both original and positional ordering as encountered various smectic phases. Toward that end, several versions of DFT have been proposed recently.[238,239] Using a nonlocal density functional for the free energy of effective hard spheres in the Parson–Lee model, Somoza and Tarazona[240] predicted first- and second-order phase transitions among nematic, smectic-A, and smectic-C phases in hard spherocylinders. Figure 19 schematically shows the phase behavior of hard cylinders. It has been demonstrated that the Somoza–Tarazona theory is also applicable to inhomogeneous spherocylinders and their mixtures.[241-244] Application of Rosenfeld's fundamental measure theory to binary hard-platelet fluids reveals that the bulk phase diagram includes an isotropic phase, one or two nematic phases of different composition, and a columnar phase.[245]

Gay–Berne model

Liquid crystals are often divided into two basic classifications: thermotropic and lyotropic. The phase transitions of lyotropic liquid crystals mainly depend on concentration, whereas those of thermotropic liquid crystals depend on both temperature and concentration. Whereas hard spherocylinders and platelets provide a good representation of lyotropic liquid crystals, they are not useful for thermotropic liquid crystals because the attractions between these particles are not included. Much theoretical work on the phase transitions of thermotropic liquid crystals is based on the Gay–Berne model.[246-248] The interaction potential between two axially asymmetric molecules is

$$u(\mathbf{r}, \omega_1, \omega_2) = 4\varepsilon(\hat{\mathbf{r}}, \omega_1, \omega_2) \times \left\{ \left[\frac{\sigma_0}{r - \sigma(\hat{\mathbf{r}}, \omega_1, \omega_2) + \sigma_0} \right]^{12} - \left[\frac{\sigma_0}{r - \sigma(\mathbf{r}, \omega_1, \omega_2) + \sigma_0} \right]^{6} \right\} \tag{23}$$

Equation 23 can be understood as an extension of the Lennard–Jones potential. The vector $\mathbf{r} = \mathbf{r}_2 - \mathbf{r}_1$ separates the centers of mass of two molecules with orientations ω_1 and ω_2; $\hat{\mathbf{r}} = \mathbf{r}/|\mathbf{r}|$ is a unit vector, and $\varepsilon(\hat{\mathbf{r}}, \omega_1, \omega_2)$ and $\sigma(\hat{\mathbf{r}}, \omega_1, \omega_2)$ are angle-dependent energy and length functions, respectively.[247] Because the Gay–Berne potential includes anisotropic repulsive and attractive components, it provides a benchmark model for

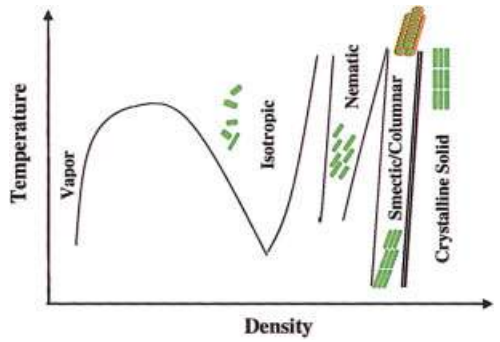

Figure 20. Liquid crystals in the Gay–Berne model predicted by DFT.

[Color figure can be viewed in the online issue, which is available at www.interscience.wiley.com.]

thermotropic liquid crystals that form a large variety of partially ordered phases.

As schematically shown in Figure 20, a simple version of DFT, derived from the virial expansion of the excess Helmholtz energy functional, is capable of describing uniform isotropic vapor and liquid phases, nematic phases, and layered smectic phases of the Gay–Berne model within a single theoretical framework.[246] The phase diagram includes isotropic-to-nematic and nematic-to-columnar phase transitions when the aspect ratio is small and the nematic phase disappears beyond a critical aspect ratio.[247] Although the transitions among vapor, isotropic liquid, and crystalline solid resemble those corresponding to simple fluids, several ordered structures appear between isotropic liquid and solid phases. In addition to nematic and smectic phases, the phase diagram of the Gay–Berne model includes a columnar phase where disk-like molecules assemble into columns with a two-dimensional spatial periodicity.

The numerical details for the application of DFT to liquid crystals are necessarily more complicated than those for simple fluids because of the higher dimensional integrations. Fortunately, the computational cost becomes of less concern compared to that of Onsager's era when a numerical solution could be obtained only by polynomial expansions. Whereas bulk phase behavior of liquid crystals has been the major focus of most DFT calculations reported in the literature, DFT is equally applicable to phase transitions of liquid crystals at inhomogeneous conditions.[249] More reports for such conditions are expected in the near future.[250,251]

Structured Soft Materials and Composites

Synthesis of materials with precisely controlled microstructure has been a hallmark of modern materials science. An outstanding example is the use of block copolymers that have been tailored for applications ranging from the exotic to such everyday materials as removable adhesive pads and the soles of running shoes. Unlike conventional crystalline materials that exhibit order at the atomic or molecular levels, structure ordering in block copolymer systems is mostly induced by microscopic phase segregation of chemically distinct segments that are covalently linked together. Such microscopic phase separations have been successfully described by the polymer self-consistent field theory.[252]

Classical DFT shares a number of similarities with the polymer self-consistent field theory except that, as in molecular simulations, DFT follows the chemical topology of polymeric molecules and specific intermolecular interactions. DFT is able not only to reproduce the morphologies of block copolymer thin films predicted by self-consistent field calculations but also to resolve the segmental detailed packing structures near the interface.[253,254] In addition to segmental/level details, DFT has the advantage of explicitly accounting for the compressibility and local segmental packing effects that are missed in a typical self-consistent field theory.

In recent years, block copolymers have been used as useful templates for fabrication of nanostructured materials.[255-257] Nanoparticle–copolymer hybrids combine the unique magnetic, electronic, catalytic, and spectroscopic features of semiconductor or metallic colloids with the flexibility, solubility, and processibility of polymers, promising for development of the next-generation catalysts, membranes, and optoelectrical devices. Controlled synthesis of such materials for tailored applications requires good understanding of how copolymer chemical structures, molecular weight, and composition, and the characteristics of nanoparticles influence microscopic morphology and phase behavior. Toward that end, the self-consistent field theory has been extended to polymer and nanoparticle mixtures by including DFT to account for the excluded-volume effect of nanoparticles.[258,259] According to the hybrid theory, the total Helmholtz energy functional for a system containing AB block copolymers and neutral nanoparticles is given by

$$F = \frac{N}{2V}\int d\mathbf{r}\sum_{i\neq j}\phi_i(\mathbf{r})\phi_j(\mathbf{r})\chi_{ij} - \frac{1}{V}\int d\mathbf{r}\sum_i \phi_i(\mathbf{r})w_i(\mathbf{r}) + (1-\phi_P)\ln[V(1-\phi_P)/Q_d] + \phi_P/\alpha\ln(V\phi_P/\alpha Q_P) + 1/V\int d\mathbf{r}\rho_P(\mathbf{r})\Phi_{hs}[\bar{\phi}_P(\mathbf{r})] \quad (24)$$

where N is the degree of polymerization of the block copolymer, V is the total volume, $\phi_i(\mathbf{r})$ represents a local volume fraction with subscript i denoting a segment A or B or a nanoparticle. The first two terms on the right-hand side of Eq. 24 account for the two-body mean-field attractive energy and the free energy arising from the self-consistent field, respectively; the next two terms stand for the free energy of a single copolymer molecule (d) and a nanoparticle (P), respectively, where Q stands for the single-molecule (particle) partition function. The parameter α denotes the particle-to-diblock volume ratio. Finally, the last term in Eq. 24 comes from the excluded-volume effect of nanoparticles, represented by the DFT of Tarazona.[132] This hybrid theory is able to capture a rich variety of mesostructures in particle–block copolymer mixtures, thereby enabling the fabrication of novel composite architectures by design.[260] Compared to molecular simulations, the hybrid DFT approach bears important advantages of numerical efficiency because of its simplicity. It provides useful insights for controlling the structures of block–copolymer–particle composites. Although application of the local incompressibility condition to a continuous model is questionable, this drawback can be overcome by taking into account the

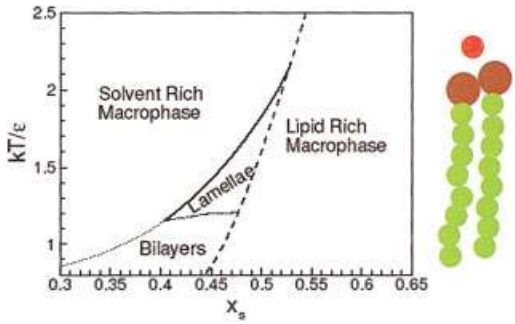

Figure 21. Phase diagram of lipid bilayers predicted by DFT.[272]

As shown above, the lipid molecules are represented by freely joined spherical beads and solvent molecules by Lennard–Jones spheres. The tail–solvent and tail–head interactions are purely repulsive, whereas the solvent-head interactions are attractive. x_s is the number fraction of solvent beads, that is, the number of solvent molecules divided by the total number of solvent and lipid beads. ε is the Lennard–Jones energy parameter for the pair interaction between lipid heads or solvent molecules. [Color figure can be viewed in the online issue, which is available at www.interscience.wiley.com.]

characteristics of both nanoparticles and block copolymers within a truly self-consistent DFT.

Molecular Self-Assembly

Amphiphilic molecules (such as surfactants) may self-organize into a variety of intriguing ordered structures in a solution. The self-assembly processes have been of prime scientific interest for decades. Applications include formation of vesicles or liposomes as carriers of therapeutic agents and as simplified models for biological membranes.[204]

Early research in the self-assembly of amphiphilic molecules has been heavily influenced by a phenomenological theory first proposed by Tanford for the formation of spherical micelles.[261] This seminal work was later extended by Nagarajan and Ruckenstein,[262] Israelachvili,[263] Blankschtein,[264] and others to more sophisticated models of self-assembly for representing the formations of micelles, bilayers, vesicles, and microemulsions. These phenomenological theories have proved useful as rules of thumb for experimental design of many amphiphilic systems including those containing lipid molecules and block copolymers.

Classical DFT has also been used to study structure ordering in amphiphilic systems for a number of years.[265-270] The basic idea is that the organized microscopic structures satisfy a local minimum of the grand potential energy, which can be described in terms of the density-functional formulism. Based on coarse-grained models of amphiphilic molecules, DFT is able to represent not only the conditions required for micellization but also the microscopic structures of spherical micelles, vesicles, and bilayer membranes made of either one-component or multicomponent amphiphiles. In addition, DFT has also been used to study the organization of amphiphilic molecules at liquid–vapor and liquid–solid interfaces. Whereas early applications of DFT emphasized the qualitative "global" phase diagram of amphiphilic systems and the microscopic origin of membrane elastic constants, DFT is also applicable to more realistic models of amphiphiles including mixed ionic surfactants and lipid bilayers.[271,272] To illustrate, Figure 21 shows a phase diagram for a coarse-grained model of lipid solutions predicted by DFT.[272] The curves denote various coexistence lines among lipid-rich and solvent-rich macrophases, and bilayers and lamellar microphases. Although only planar symmetry is considered, the DFT captures compressibility and packing effects of flexible lipid molecules in a solvent and is naturally applicable to both micro- and macrophases.

Summary and Outlook

As a generic method in statistical mechanics, classical *density functional theory* (DFT) offers a powerful alternative to a variety of conventional theoretical methods and molecular simulations for linking microscopic properties of chemical systems to the structural and thermodynamic properties. The practical value of DFT is reflected not only by its generality but also by its versatility for solving problems that may not be attained by conventional theories. This review gives some specific examples where DFT is more informative compared to conventional methods. There is no need to apply DFT to problems where conventional theories are sufficient, as in typical vapor–liquid or liquid–liquid phase-equilibrium calculations that can be satisfactorily achieved by using classical equations of state or local-composition models. However, we cannot expect these conventional theories to be applicable to interfacial properties and to phase transitions that occur in a confined geometry or that concern structure formation as in solubilization of copolymers in a liquid or in supercritical carbon dioxide.[273] The usefulness of many phenomenological theories has been well established and they remain valuable as long as the underlying approximations can be adequately justified for a specific problem.

Future applications of DFT depend on continuing progress toward more faithful representation of density functionals reflecting molecular-level interactions and, more important, clever implementation methods such as the curvature expansions of local density profiles.[274] Further, more efficient numerical algorithms are required to solve multidimensional density profiles. Although much current work in the literature concerns relatively simple models with emphasis on the performance of various versions of density functionals for representing the qualitative or semiquantitative physiochemical properties in the bulk or under confinement, we anticipate that, once more realistic intermolecular force fields and reliable expressions of the excess Helmholtz energy functionals are established, DFT will be useful for more complex systems, in particular for those related to material fabrication, environmental protection, and biomolecular engineering. Important advances are already emerging in applications of DFT to crystal nucleation and growth,[29] aerosol formation,[275] structures of copolymers and composites,[99,260] transport processes through ion channels,[27] protein folding and aggregation in "crowded" environment,[28] polymers for surface protection and antifouling,[201] and self-assembly of lipid bilayers.[272,276,277] Future applications of DFT will be most promising by integrating fundamental understandings from theoretical calculations with engineering practices for development of environmentally friendly chemical and biological processes and products.

DFT is useful not only for describing equilibrium phenomena as discussed in this review. Extension of DFT to nonequi-

librium systems and kinetics/dynamics of microscopic processes is now also well advanced. However, similar to classical thermodynamics, DFT provides *only* a methodology. Whereas the mathematical framework is exact, its successful implementation depends first on realistic molecular models and, more important, on reliable expressions of the excess Helmholtz energy functional. For most systems of interest for materials and biological applications, we have neither truly accurate molecular models nor exact Helmholtz energy functionals. Fortunately, chemical engineers have long recognized that, for practical applications, a theoretical model need not be exact. For broad chemical engineering applications, we also recognize the value of simple models that contain the essential physics of natural phenomena, and semiempirical quantitative models that provide reliable correlation of physiochemical properties. Toward that end, DFT provides a useful methodology.

Acknowledgments

The author is indebted to John Prausnitz for inspiration and assistance leading to this work and for numerous fruitful discussions. The author also benefited from insightful comments and suggestions from Marc-Olivier Coppens, University of Delft; Marcus Muller, University of Wisconsin; and Roland Roth, Max-Planck Institute at Stuttgart. Special thanks to Alexander Neimark, who kindly provided me with Figure 9. This project was supported by the National Science Foundation.

Literature Cited

1. Chandler D. *Introduction to Modern Statistical Mechanics.* New York, NY: Oxford Univ. Press, 1987.
2. Hansen JP, McDonald IR. *Theory of Simple Liquids.* 2nd Edition. London/New York: Academic Press; 1990.
3. Deem MW. Recent contributions of statistical mechanics in chemical engineering. *AIChE J.* 1998;44:2569-2596.
4. Chakraborty AK, ed. Molecular modeling and theory chemical engineering. In: Wei J, ed. *Advances in Chemical Engineering*. Vol. 28. San Diego, CA: Academic Press; 2001.
5. Debenedetti PG. *Metastable Liquids: Concepts and Principles.* Princeton, NJ: Princeton Univ. Press; 1996.
6. Orbey H, Sandler SI. *Modeling Vapor–Liquid Equilibria: Cubic Equations of State and Their Mixing Rules.* New York, NY: Cambridge Univ. Press; 1998.
7. Prausnitz JM, Tavares FW. Thermodynamics of fluid-phase equilibria for standard chemical engineering operations. *AIChE J.* 2004;50: 739-761.
8. Ruthven DM. *Principles of Adsorption and Adsorption Processes.* New York, NY: Wiley; 1984.
9. Sloan ED. *Clathrate Hydrates of Natural Gases.* 2nd Edition, revised/expanded. New York, NY: Marcel Dekker; 1998.
10. de Pablo JJ, Escobedo FA. Molecular simulations in chemical engineering: Present and future. *AIChE J.* 2002;48:2716-2721.
11. Keil FJ, Krishna R, Coppens MO. Modeling of diffusion in zeolites. *Rev Chem Eng.* 2000;16:71-197.
12. Lee LL. *Molecular Thermodynamics of Nonideal Fluids.* Boston, MA: Butterworths; 1988.
13. Schweizer KS, Curro JG. Integral equation theories of the structure, thermodynamics, and phase transitions of polymer fluids. *Adv Chem Phys.* 1997;98:1-142.
14. Fredrickson GH, Ganesan V, Drolet F. Field-theoretic computer simulation methods for polymers and complex fluids. *Macromolecules.* 2002;35:16-39.
15. Wang Z. Morphology, fluctuation, metastability, and kinetics in ordered block copolymers. In: Chakraborty A, ed. *Molecular Modeling and Theory in Chemical Engineering.* San Diego, CA: Academic Press; 2001:439-464.
16. Theodorou DN. Polymers at surfaces and interfaces. In: Dunweg B, ed. *Computer Simulations of Surfaces and Interfaces.* Dordrecht, The Netherlands: Kluwer Academic; 2003:329-419.
17. Davis HT. *Statistical Mechanics of Phases, Interfaces, and Thin Films.* New York, NY: VCH; 1996.
18. Oxtoby DW. Density functional methods in the statistical mechanics of materials. *Annu Rev Mater Res.* 2002;32:39-52.
19. Sengers JV, ed. Equations of state for fluids and fluid mixtures. *Experimental Thermodynamics*. 1st Edition, Vol. 5. Amsterdam, The Netherlands: Elsevier; 2000;xix:885.
20. Muller EA, Gubbins KE. Molecular-based equations of state for associating fluids: A review of SAFT and related approaches. *Ind Eng Chem Res.* 2001;40:2193-2211.
21. Trout B. Car–Parrinello methods in chemical engineering: Their scope and potential. In: Chakraborty A, ed. *Molecular Modeling and Theory in Chemical Engineering.* San Diego, CA: Academic Press; 2001:353-395.
22. Evans R. Density functionals in the theory of nonuniform fluids. In: Henderson D, ed. *Fundamentals of Inhomogeneous Fluids.* New York, NY: Marcel Dekker; 1992:85-175.
23. Lowen H. Density functional theory: From statics to dynamics. *J Phys Condens Matter.* 2003;15:V1-V3.
24. Frink LJD, Salinger AG, Sears MP, Weinhold JD, Frischknecht AL. Numerical challenges in the application of density functional theory to biology and nanotechnology. *J Phys Condens Matter.* 2002;14: 12167-12187.
25. Ebner C, Saam WF, Stroud D. Density-functional theory of simple classical fluids. I. Surfaces. *Phys Rev A.* 1976;14:2264-2273.
26. Goulding D, Hansen JP, Melchionna S. Size selectivity of narrow pores. *Phys Rev Lett.* 2000;85:1132-1135.
27. Gillespie D, Nonner W, Eisenberg RS. Coupling Poisson–Nernst–Planck and density functional theory to calculate ion flux. *J Phys Condens Matter.* 2002;14:12129-12145.
28. Kinjo AR, Takada S. Competition between protein folding and aggregation with molecular chaperones in crowded solutions: Insight from mesoscopic simulations. *Biophys J.* 2003;85:3521-3531.
29. Oxtoby DW. Crystal nucleation in simple and complex fluids. *Philos Trans R Soc Lond A Math Phys Eng Sci.* 2003;361:419-427.
30. Fraaije J. Dynamic density-functional theory for microphase separation kinetics of block-copolymer melts. *J Chem Phys*. 1993;99:9202-9212.
31. Marconi UMB, Tarazona P. Dynamic density functional theory of fluids. *J Phys Condens Matter.* 2000;12:A413-A418.
32. Shen VK, Debenedetti PG. Density-functional study of homogeneous bubble nucleation in the stretched Lennard–Jones fluid. *J Chem Phys*. 2001;114:4149-4159.
33. Hohenberg P, Kohn W. Inhomogeneous electron gas. *Phys Rev.* 1964;136:B864-B871.
34. Mermin ND. Thermal properties of the inhomogeneous electron gas. *Phys Rev.* 1965;127:A1441-A1443.
35. Kohn W, Sham LJ. Self-consistent equations including exchange and correlation effects. *Phys Rev.* 1965;140:A1133-A1138.
36. van der Waals JD. Thermodynamische theorie der capillariteit in de onderstelling van continue dichtheidsverandering. *Verh K Akad Wet Amsterdam*. 1893;1:8.
37. Rowlinson JS. J. D. van der Waals: On the continuity of the gaseous and liquid states. In: Rowlinson JS, ed. *Studies in Statistical Mechanics.* New York, NY: Elsevier Science; 1988:121.
38. Onsager L. The effects of shape on the interaction of colloidal particles. *Ann NY Acad Sci.* 1949;51:627-659.
39. de Gennes PG, Prost J. *The Physics of Liquid Crystals.* New York, NY: Oxford Univ. Press; 1993.
40. Cahn JW. Critical point wetting. *J Chem Phys*. 1977;66:3667-3672.
41. Rutledge JE, Taborek P. Prewetting phase diagram of 4He on cesium. *Phys Rev Lett.* 1992;69:937-940.
42. Yethiraj A, Woodward CE. Monte Carlo density functional theory of nonuniform polymer melts. *J Chem Phys*. 1995;102:5499-5505.
43. Chandler D, Weeks JD, Andersen HC. Van der Waals picture of liquids, solids, and phase transformations. *Science.* 1983;220:787-794.
44. Reiss H, Frisch HL, Lebowitz JL. Statistical mechanics of rigid spheres. *J Chem Phys*. 1959;31:369-380.
45. Percus JK, Yevick GJ. Analysis of classical statistical mechanics by means of collective coordinates. *Phys Rev.* 1958;110:1.
46. Boublik T. Hard-sphere equation of state. *J Chem Phys*. 1970;53: 471-472.
47. Mansoori GA, Carnahan NF, Starling KE, Leland TW Jr. Equilibrium

thermodynamic properties of the mixture of hard spheres. *J Chem Phys*. 1971;54:1523-1525.
48. Cuesta JA, Martinez-Raton Y, Tarazona P. Close to the edge of fundamental measure theory: A density functional for hard-sphere mixtures. *J Phys Condens Matter.* 2002;14:11965-11980.
49. Rosenfeld Y. Free-energy model for the inhomogeneous hard-sphere fluid mixture and density-functional theory of freezing. *Phys Rev Lett.* 1989;63:980-983.
50. Rosenfeld Y. Free energy model for the inhomogeneous hard-body fluid—Application of the Gauss–Bonnet theorem. *Mol Phys.* 1995; 86:637-647.
51. Oversteegen SM, Roth R. General methods for free-volume theory. *J Chem Phys.* 2005;122:214502.
52. Yu YX, Wu JZ. Structures of hard sphere fluids from a modified fundamental measure theory. *J Chem Phys*. 2002;117:10156-10164.
53. Roth R, Evans R, Lang A, Kahl G. Fundamental measure theory for hard-sphere mixtures revisited: The White Bear version. *J Phys Condens Matter.* 2002;14:12063-12078.
54. Tang YP, Wu JZ. Modeling inhomogeneous van der Waals fluids using an analytical direct correlation function. *Phys Rev E*. 2004;70: 011201.
55. Tang YP, Lu BCY. A new solution of the Ornstein–Zernike equation from the perturbation theory. *J Chem Phys*. 1993;99:9828-9835.
56. Tang YP, Lu BCY. First-order radial distribution functions based on the mean spherical approximation for square-well, Lennard–Jones, and Kihara fluids. *J Chem Phys*. 1994;100:3079-3084.
57. Tang YP, Lu BCY. Analytical solution of the Ornstein–Zernike equation for mixtures. *Mol Phys.* 1995;84:89-103.
58. Tang YP, Lu BCY. Analytical representation of the radial distribution function for classical fluids. *Mol Phys.* 1997;90:215-224.
59. Tang YP, Lu BCY. On the mean spherical approximation for the Lennard–Jones fluid. *Fluid Phase Equilib.* 2001;190:149-158.
60. Tang YP. On the first-order mean spherical approximation. *J Chem Phys*. 2003;118:4140-4148.
61. Li ZD, Cao DP, Wu JZ. Density functional theory and Monte Carlo simulations for the surface structure and correlation functions of freely jointed Lennard–Jones fluids. *J Chem Phys*. 2005;122:174708.
62. Pratt LR, Chandler D. Interaction site cluster series for the Helmholtz free energy and variational principle for chemical equilibria and intramolecular structures. *J Chem Phys*. 1977;66:147-151.
63. Wertheim MS. Fluids with highly directional attractive forces. I. Statistical thermodynamics. *J Stat Phys.* 1984;35:19-34.
64. Chapman WG, Jackson G, Gubbins KE. Phase equilibria of associating fluids: Chain molecules with multiple bonding sites. *Mol Phys.* 1988;65:1057-1079.
65. Segura CJ, Chapman WG, Shukla KP. Associating fluids with four bonding sites against a hard wall: Density functional theory. *Mol Phys.* 1997;90:759-771.
66. Segura CJ, Vakarin EV, Chapman WG, Holovko MF. A comparison of density functional and integral equation theories vs Monte Carlo simulations for hard sphere associating fluids near a hard wall. *J Chem Phys*. 1998;108:4837-4848.
67. Segura CJ, Zhang J, Chapman WG. Binary associating fluid mixtures against a hard wall: Density functional theory and simulation. *Mol Phys.* 2001;99:1-12.
68. Yu YX, Wu JZ. A fundamental-measure theory for inhomogeneous associating fluids. *J Chem Phys*. 2002;116:7094-7103.
69. Paricaud P, Galindo A, Jackson G. Recent advances in the use of the SAFT approach in describing electrolytes, interfaces, liquid crystals and polymers. *Fluid Phase Equilib.* 2002;194:87-96.
70. Tripathi S, Chapman WG. A density functional approach to chemical reaction equilibria in confined systems: Application to dimerization. *J Chem Phys*. 2003;118:7993-8003.
71. Pizio O, Patrykiejew A, Sokolowski S. Evaluation of liquid–vapor density profiles for associating fluids in pores from density-functional theory. *J Chem Phys*. 2000;113:10761-10767.
72. Malo BM, Huerta A, Pizio O, Sokolowski S. Phase behavior of associating two- and four-bonding sites Lennard–Jones fluid in contact with solid surfaces. *J Phys Chem B.* 2000;104:7756-7763.
73. Huerta A, Pizio O, Bryk P, Sokolowski S. Application of the density functional method to study phase transitions in an associating Lennard–Jones fluid adsorbed in energetically heterogeneous slit-like pores. *Mol Phys.* 2000;98:1859-1869.
74. Li ZD, Wu JZ. Density-functional theory for the structures and thermodynamic properties of highly asymmetric electrolyte and neutral component mixtures. *Phys Rev E*. 2004;70:031109.
75. Gillespie D, Nonner W, Eisenberg RS. Density functional theory of charged, hard-sphere fluids. *Phys Rev E*. 2003;68:031503.
76. Patra CN, Yethiraj A. Density functional theory for the distribution of small ions around polyions. *J Phys Chem B.* 1999;103:6080-6087.
77. Henderson D, Bryk P, Sokolowski S, Wasan DT. Density-functional theory for an electrolyte confined by thin charged walls. *Phys Rev E.* 2000;61:3896-3903.
78. Boda D, Henderson D, Teran LMY, Sokolowski S. The application of density functional theory and the generalized mean spherical approximation to double layers containing strongly coupled ions. *J Phys Condens Matter.* 2002;14:11945-11954.
79. Blum L. Mean spherical model for asymmetric electrolytes. 1. Method of solution. *Mol Phys.* 1975;35:299.
80. Tang ZX, Scriven LE, Davis HT. Interactions between primitive electrical double-layers. *J Chem Phys*. 1992;97:9258-9266.
81. Yu YX, Wu JZ, Gao GH. Density-functional theory of spherical electric double layers and zeta potentials of colloidal particles in restricted-primitive-model electrolyte solutions. *J Chem Phys*. 2004; 120:7223-7233.
82. Chandler D, McCoy JD, Singer SJ. Density functional theory of nonuniform polyatomic systems. I. General formulation. *J Chem Phys*. 1986;85:5971-5976.
83. Phan S, Kierlik E, Rosinberg ML, Yethiraj A, Dickman R. Perturbation density functional theory and Monte Carlo simulations for the structure of hard triatomic fluids in slitlike pores. *J Chem Phys*. 1995;102:2141-2150.
84. Yethiraj A. Polymer melts at solid surfaces. *Adv Chem Phys.* 2002; 121:89-139.
85. Patra CN, Yethiraj A. Density functional theory for nonuniform polymers: Accurate treatment of the effect of attractive interactions. *J Chem Phys*. 2003;118:4702-4706.
86. Yethiraj A. Density functional theory of polymers: A Curtin–Ashcroft type weighted density approximation. *J Chem Phys*. 1998;109: 3269-3275.
87. Muller M, MacDowell LG, Yethiraj A. Short chains at surfaces and interfaces: A quantitative comparison between density-functional theories and Monte Carlo simulations. *J Chem Phys*. 2003;118:2929-2940.
88. Tripathi S, Chapman WG. Microstructure and thermodynamics of inhomogeneous polymer blends and solutions. *Phys Rev Lett.* 2005; 94:087801.
89. Kierlik E, Rosinberg ML. A perturbation density-functional theory for polyatomic fluids. 1. Rigid molecules. *J Chem Phys*. 1992;97: 9222-9239.
90. Hooper JB, McCoy JD, Curro JG, van Swol F. Density functional theory of simple polymers in a slit pore. III. Surface tension. *J Chem Phys*. 2000;113:2021-2024.
91. Hooper JB, McCoy JD, Curro JG. Density functional theory of simple polymers in a slit pore. I. Theory and efficient algorithm. *J Chem Phys*. 2000;112:3090-3093.
92. Hooper JB, Pileggi MT, McCoy JD, Curro JG, Weinhold JD. Density functional theory of simple polymers in a slit pore. II. The role of compressibility and field type. *J Chem Phys*. 2000;112:3094-3103.
93. Schweizer KS, Curro JG. Integral equation theories of the structure, thermodynamics, and phase transitions of polymer fluids. *Adv Chem Phys.* 1997;98:1-142.
94. Woodward CE. A density functional theory for polymers—Application to hard chain hard-sphere mixtures in slitlike pores. *J Chem Phys*. 1991;94:3183-3191.
95. Woodward CE, Yethiraj A. Density functional theory for inhomogeneous polymer solutions. *J Chem Phys*. 1994;100:3181-3186.
96. Yu YX, Wu JZ. Density functional theory for inhomogeneous mixtures of polymeric fluids. *J Chem Phys*. 2002;117:2368-2376.
97. Cao DP, Wu JZ. Density funtional theory for semi-flexible and cyclic polyatomic fluids. *J Chem Phys*. 2004;121:4210-4220.
98. Cao DP, Wu JZ. Surface-induced lamellar-lamellar phase transition of block copolymer thin films. *J Chem Phys*. 2005;122:194703.
99. Cao DP, Wu JZ. Microstructure of block copolymer near selective surfaces: Theoretical predictions and configurational-bias Monte Carlo simulations. *Macromolecules.* 2005;38:971-978.
100. Cao DP, Wu JZ. A theoretical study of cooperativity in multivalent polymers for colloidal stabilization. *Langmuir*. 2005;21:9786-9791.

101. Krantz WB, Wasan DT, Jain RK. Thin liquid film phenomena. Proc of American Chemical Society Meeting, American Institute of Chemical Engineers (AIChE), Interfacial Phenomena Technical Program Committee, Division of Colloid and Surface Chemistry. New York, NY: AIChE; 1986.
102. Wasan DT, Payatakes A. *Interfacial Phenomena in Enhanced Oil Recovery.* New York, NY: American Institute of Chemical Engineers; 1982.
103. Wasan DT, Ginn ME, Shah DO. *Surfactants in Chemical/Process Engineering.* New York, NY: Marcel Dekker; 1988.
104. Edwards DA, Brenner H, Wasan DT. *Interfacial Transport Processes and Rheology.* Boston, MA: Butterworth-Heinemann; 1991.
105. Fu D, Wu J. Vapor–liquid equilibria and interfacial tensions of associating fluids within a density functional theory. *Ind Eng Chem Res.* 2005;44:1120-1128.
106. White JA, Zhang S. Renormalization group theory for fluids. *J Chem Phys*. 1993;99:2012-2019.
107. Kierlik E, Phan S, Rosinberg ML. Density-functional theory for nonuniform polyatomic fluids. *ACS Symp Ser.*1996:212-228.
108. Bryk P, Sokolowski S. Bulk and interfacial properties of binary polymer mixtures. *J Chem Phys*. 2004;120:8299-8306.
109. Dagama MMT, Evans R, Sluckin TJ. The structure and surface-tension of the liquid–vapor interface of a model of a molten-salt. *Mol Phys.* 1980;41:1355-1372.
110. Gonzalez-Melchor M, Alejandre J, Bresme F. Surface tension of the restrictive primitive model for ionic liquids. *Phys Rev Lett*. 2003;90: 135506.
111. Groh B, Evans R, Dietrich S. Liquid–vapor interface of an ionic fluid. *Phys Rev E.* 1998;57:6944-6954.
112. Napari I, Laaksonen A, Strey R. Density-functional studies of amphiphilic binary mixtures. I. Phase behavior. *J Chem Phys*. 2000;113: 4476-4479.
113. Dee GT, Sauer BB. The surface tension of polymer liquids. *Adv Phys.* 1998;47:161-205.
114. Napari I, Laaksonen A, Talanquer V, Oxtoby DW. A density functional study of liquid–liquid interfaces in partially miscible systems. *J Chem Phys*. 1999;110:5906-5912.
115. Bucior K, Patrykiejew A, Sokolowski S, Pizio O. Liquid–liquid interface in a binary mixture of associating fluids exhibiting a closed-loop immiscibility. *Mol Phys.* 2003;101:2233-2240.
116. Patrykiejew A, Pizio O, Pusztai L, Sokolowski S. Effects of slit-like pore confinement on the closed loop immiscibility in symmetric binary model mixtures. *Mol Phys.* 2003;101:2219-2223.
117. Kierlik E, Fan Y, Monson PA, Rosinberg ML. Liquid–liquid equilibrium in a slit pore–Monte Carlo simulation and mean field density functional theory. *J Chem Phys*. 1995;102:3712-3719.
118. Bryk P. Demixing in athermal mixtures of colloids and excluded-volume polymers from density functional theory. *J Chem Phys*. 2005;122:064902.
119. Louis AA, Bolhuis PG, Finken R, Krakoviack V, Meijer EJ, Hansen JP. Coarse-graining polymers as soft colloids. *Physica A* 2002;306: 251-261.
120. Archer AJ, Likos CN, Evans R. Binary star-polymer solutions: Bulk and interfacial properties. *J Phys Condens Matter.* 2002;14:12031-12050.
121. Tarazona P, Chacon E, Velasco E. The Fisher–Widom line for systems with low melting temperature. *Mol Phys.* 2003;101:1595-1603.
122. McDonald AJ, Allen MP, Schmid F. Surface tension of the isotropic–nematic interface. *Phys Rev E.* 2001;6301:010701.
123. Bisio PD, Cartledge JG, Keesom WH, Radke CJ. Molecular-orientation of aqueous surfactants on a hydrophobic solid. *J Colloid Interface Sci.* 1980;78:225-234.
124. Stoyanov SD, Rehage H, Paunov VN. Novel surface tension isotherm for surfactants based on local density functional theory. *Phys Rev Lett*. 2003;91:086102.
125. Mecke KR, Dietrich S. Effective Hamiltonian for liquid–vapor interfaces. *Phys Rev E.* 1999;59:6766-6784.
126. Fradin C, Braslau A, Luzet D, Smilgies D, Alba M, Boudet N, Mecke K, Daillant J. Reduction in the surface energy of liquid interfaces at short length scales. *Nature.* 2000;403:871-874.
127. Dabrowski A. Adsorption—From theory to practice. *Adv Colloid Interface Sci.* 2001;93:135-224.
128. Gelb LD, Gubbins KE, Radhakrishnan R, Sliwinska-Bartkowiak M. Phase separation in confined systems. *Rep Prog Phys.* 1999;62:1573-1659.
129. Varga S, Boda D, Henderson D, Sokolowski S. Density functional theory and the capillary evaporation of a liquid in a slit. *J Colloid Interface Sci.* 2000;227:223-226.
130. Trokhymchuk A, Henderson D, Sokolowski S. Local density of overlapping spheres near a hard wall: A density functional approach. *Phys Lett A.* 1995;209:317-320.
131. Balbuena PB, Gubbins KE. Theoretical interpretation of adsorption behavior of simple fluids in slit pores. *Langmuir.* 1993;9:1801-1814.
132. Tarazona P. Free energy density functional for hard spheres. *Phys Rev A Gen Phys* 1985;31:2672-2679.
133. Neimark AV, Ravikovitch PI, Vishnyakov A. Bridging scales from molecular simulations to classical thermodynamics: Density functional theory of capillary condensation in nanopores. *J Phys Condens Matter.* 2003;15:347-365.
134. Ravikovitch PI, Neimark AV. Characterization of micro- and mesoporosity in SBA-15 materials from adsorption data by the NLDFT method. *J Phys Chem B.* 2001;105:6817-6823.
135. Lastoskie CM, Gubbins KE. Characterization of porous materials using molecular theory and simulation. In: Chakraborty AK, ed. *Molecular Modeling and Theory in Chemical Engineering.* San Diego, CA: Academic Press; 2001.
136. Sweatman MB. Analysis of free energy functional density expansion theories. *Mol Phys.* 2000;98:573-581.
137. Patra CN, Ghosh SK. Structure of nonuniform fluid mixtures: A self-consistent density-functional approach. *J Chem Phys*. 2002;117: 8933-8937.
138. Zhou S, Ruckenstein E. A new density functional approach to non-uniform Lennard–Jones fluids. *J Chem Phys*. 2000;112.
139. Sliwinska-Bartkowiak M, Sikorski R, Sowers SL, Gelb LD, Gubbins KE. Phase separations for mixtures in well-characterized porous materials: Liquid–liquid transitions. *Fluid Phase Equilib.* 1997;136: 93-109.
140. Patrykiejew A, Pizio O, Sokolowski S. Demixing transitions in a binary Gaussian-core fluid confined in narrow slit-like pores. *Mol Phys.* 2004;102:801-810.
141. Malo BM, Pizio O, Patrykiejew A, Sokolowski S. Adsorption and phase transitions in a two-site associating Lennard–Jones fluid confined to energetically heterogeneous slit-like pores; application of the density functional method. *J Phys Condens Matter.* 2001;13:1361-1379.
142. Brovchenko I, Geiger A, Oleinikova A. Water in nanopores. I. Coexistence curves from Gibbs ensemble Monte Carlo simulations. *J Chem Phys*. 2004;120:1958-1972.
143. Bonn D, Ross D. Wetting transitions. *Rep Prog Phys.* 2001;64:1085-1163.
144. Muller M, MacDowell LG. Wetting of polymer liquids: Monte Carlo simulations and self-consistent field calculations. *J Phys Condens Matter.* 2003;15:R609-R653.
145. Brochard-Wyart F, Dimeglio JM, Quere D, de Gennes PG. Spreading of nonvolatile liquids in a continuum picture. *Langmuir*. 1991;7:335-338.
146. Bertrand E, Dobbs H, Broseta D, Indekeu J, Bonn D, Meunier J. First-order and critical wetting of alkanes on water. *Phys Rev Lett.* 2000;85:1282-1285.
147. Ebner C, Saam WF. New phase-transition phenomena in thin argon films. *Phys Rev Lett.* 1977;38:1486-1489.
148. Kellay H, Bonn D, Meunier J. Prewetting in a binary liquid mixture. *Phys Rev Lett.* 1993;71:2607-2610.
149. Sweatman MB. Weighted density-functional theory for simple fluids: Prewetting of a Lennard–Jones fluid. *Phys Rev E.* 2002;65.
150. Denesyuka NA, Hansen JP. Wetting transitions of ionic solutions. *J Chem Phys*. 2004;121:3613-3624.
151. Indekeu JO, Ragil K, Bonn D, Broseta D, Meunier J. Wetting of alkanes on water from a Cahn-type theory: Effects of long-range forces. *J Stat Phys.* 1999;95:1009-1043.
152. Nakanishi H, Fisher ME. Multicriticality of wetting, pre-wetting, and surface transitions. *Phys Rev Lett.* 1982;49:1565-1568.
153. Gonzalez A, da Gama MMT. Density functional theory of long-range critical wetting. *Phys Rev E.* 2000;62:6571-6576.
154. Vanswol F, Henderson JR. Wetting and drying transitions at a fluid–wall interface—Density-functional theory versus computer-simulation. *Phys Rev A.* 1989;40:2567-2578.

155. Vanswol F, Henderson JR. Wetting and drying transitions at a fluid–wall interface—Density-functional theory versus computer-simulation. 2. *Phys Rev A*. 1991;43:2932-2942.
156. Teletzke GF, Scriven LE, Davis HT. Wetting transitions. II. First order or second order? *J Chem Phys*. 1983;78:1431-1439.
157. Teletzke GF, Scriven LE, Davis HT. Wetting transitions: First order or second order? *J Chem Phys*. 1982;77:5794-5798.
158. Binder K. Phase transitions of polymer blends and block copolymer melts in thin films. *Adv Polym Sci.* 1999;138:1-89.
159. Geoghegan M, Krausch G. Wetting at polymer surfaces and interfaces. *Prog Polym Sci.* 2003;28:261-302.
160. Bryk P, Sokolowski S. Short chains at solid surfaces: Wetting transition from a density functional approach. *J Chem Phys*. 2004;121: 11314-11321.
161. Forsman J, Woodward CE, Freasier BC. Density functional study of wetting by polymers. I. Effects of polymer length and surface potential. *J Chem Phys*. 2002;116:4715-4722.
162. Rafai S, Bonn D, Bertrand E, Meunier J, Weiss VC, Indekeu JO. Long-range critical wetting: Observation of a critical end point. *Phys Rev Lett*. 2004;92:245701.
163. Voronov A, Shafranska O. Synthesis of chemically grafted polystyrene "brushes" and their influence on the dewetting in thin polystyrene films. *Langmuir.* 2002;18:4471-4477.
164. Voronov A, Shafranska O. Dependence of thin polystyrene films stability on the thickness of grafted polystyrene brushes. *Polymer.* 2003;44:277-281.
165. Muller M, MacDowell LG, Muller-Buschbaum P, Wunnike O, Stamm M. Nano-dewetting: Interplay between van der Waals- and short-ranged interactions. *J Chem Phys*. 2001;115:9960-9969.
166. Holyst R, Poniewierski A. Wetting on a spherical surface. *Phys Rev B.* 1987;36:5628-5630.
167. Bieker T, Dietrich S. Wetting of curved surfaces. *Physica A Stat Mech Appl.* 1998;252:85-137.
168. Bykov TV, Zeng XC. Heterogeneous nucleation on mesoscopic wettable particles: A hybrid thermodynamic/density-functional theory. *J Chem Phys*. 2002;117:1851-1868.
169. Hadjiagapiou I. Wetting on an attractive compact spherical substrate. *J Chem Phys*. 1996;105:2927-2935.
170. Henderson D, Sokolowski S, Patrykiejew A. Adsorption of fluids on colloidal particles—A density-functional approach. *Mol Phys.* 1995; 85:745-755.
171. Stillinger FH. Structure in aqueous solutions of nonpolar solutes from the standpoint of scaled-particle theory. *J Solution Chem.* 1973;2: 141-158.
172. Lum K, Chandler D, Weeks JD. Hydrophobicity at small and large length scales. *J Phys Chem B.* 1999;103:4570-4577.
173. Konig PM, Roth R, Mecke KR. Morphological thermodynamics of fluids: Shape dependence of free energies. *Phys Rev Lett*. 2004;93: 160601.
174. Tang YP, Wu JZ. Modeling inhomogeneous van der Waals systems using an analytical direct correlation function. *Phys Rev E*. 2004;70: 011201.
175. Forsman J, Jonsson B, Woodward CE, Wennerstrom H. Attractive surface forces due to liquid density depression. *J Phys Chem B.* 1997;101:4253-4259.
176. Forsman J, Woodward CE, Jonsson B. The origins of hydration forces: Monte Carlo simulations and density functional theory. *Langmuir* 1997;13:5459-5464.
177. Evans R, Henderson JR, Roth R. Nonanalytic curvature contributions to solvation free energies: Influence of drying. *J Chem Phys*. 2004; 121:12074-12084.
178. Grosberg AY, Nguyen TT, Shklovskii BI. Colloquium: The physics of charge inversion in chemical and biological systems. *Rev Modern Phys.* 2002;74:329-345.
179. Messina R, Holm C, Kremer K. Charge inversion in colloidal systems. *Comput Phys Commun.* 2002;147:282-285.
180. Wu JZ, Bratko D, Prausnitz JM. Interaction between like-charged colloidal spheres in electrolyte solutions. *Proc Natl Acad Sci USA*. 1998;95:15169-15172.
181. Decher G. Fuzzy nanoassemblies: Toward layered polymeric multicomposites. *Science.* 1997;277:1232-1237.
182. Nguyen QT, Ping ZH, Nguyen T, Rigal P. Simple method for immobilization of bio-macromolecules onto membranes of different types. *J Membr Sci.* 2003;213:85-95.
183. Radler JO, Koltover I, Salditt T, Safinya CR. Structure of DNA–cationic liposome complexes: DNA intercalation in multilamellar membranes in distinct interhelical packing regimes. *Science.* 1997; 275:810-814.
184. Tang ZX, Teran LMY, Davis HT, Scriven LE, White HS. Non-local free-energy density-functional theory applied to the electrical double layer. 1. Symmetrical electrolytes. *Mol Phys.* 1990;71:369-392.
185. Forsman J, Woodward CE, Freasier BC. Density functional study of surface forces in athermal polymer solutions with additive hard sphere interactions: Solvent effects, capillary condensation, and capillary-induced surface transitions. *J Chem Phys*. 2002;117:1915-1926.
186. Archer AJ, Evans R, Roth R, Oettel M. Solvent mediated interactions close to fluid–fluid phase separation: Microscopic treatment of bridging in a soft-core fluid. *J Chem Phys*. 2005;122:084513.
187. Archer AJ, Evans R. Solvent-mediated interactions and solvation close to fluid–fluid phase separation: A density functional treatment. *J Chem Phys*. 2003;118:9726-9746.
188. McCoy JD, Ye Y, Curro JG. Application of density functional theory to tethered polymer chains: Athermal systems. *J Chem Phys*. 2002; 117:2975-2986.
189. Forsman J, Woodward CE, Freasier BC. Density functional studies of solvation forces in hard sphere polymer solutions confined between adsorbing walls. I. Solvent effects and dependence on surface potential range. *J Chem Phys*. 2003;118:7672-7681.
190. Woodward CE, Forsman J. Density functional study of surface forces in solutions containing star-shaped polymers. *Macromolecules.* 2004; 37:7034-7041.
191. Patel N, Egorov SA. Interactions between colloidal particles in polymer solutions: A density functional theory study. *J Chem Phys*. 2004;121:4987-4997.
192. Roth R, Evans R, Dietrich S. Depletion potential in hard-sphere mixtures: Theory and applications. *Phys Rev E.* 2000;62:5360-5377.
193. Kramer T, Schweins R, Huber K. Silsesquioxane molecules and polystyrene chains as a model system for colloid—polymer mixtures in the protein limit. *Macromolecules.* 2005;38:151-159.
194. Karayiannis NC, Mavrantzas VG, Theodorou DN. A novel Monte Carlo scheme for the rapid equilibration of atomistic model polymer systems of precisely defined molecular architecture. *Phys Rev Lett*. 2002;88:105503.
195. Banaszak BJ, de Pablo JJ. A new double-rebridging technique for linear polyethylene. *J Chem Phys*. 2003;119:2456-2462.
196. Bolhuis PG, Meijer EJ, Louis AA. Colloid–polymer mixtures in the protein limit. *Phys Rev Lett*. 2003;90:068304.
197. Doxastakis M, Chen YL, de Pablo JJ. Potential of mean force between two nanometer-scale particles in a polymer solution. *J Chem Phys*. 2005;123:034901.
198. Tirrell M, Kokkoli E, Biesalski M. The role of surface science in bioengineered materials. *Surf Sci.* 2002;500:61-83.
199. Castner DG, Ratner BD. Biomedical surface science: Foundations to frontiers. *Surf Sci.* 2002;500:28-60.
200. de Gennes PG. Conformations of polymers attached to an interface. *Macromolecules.* 1980;13:1069.
201. Szleifer I. Protein adsorption on surfaces with grafted polymers: A theoretical approach. *Biophys J.* 1997;72:595-612.
202. McCoy JD, Ye Y, Curro JG. Application of density functional theory to tethered polymer chains: Athermal systems. *J Chem Phys*. 2003; 117:2975-2986.
203. Ye Y, McCoy JD, Curro JG. Application of density functional theory to tethered polymer chains: Effect of intermolecular attractions. *J Chem Phys*. 2003;119:555-564.
204. Auguste DT, Prud'homme RK, Ahl PL, Meers P, Kohn J. Association of hydrophobically-modified poly(ethylene glycol) with fusogenic liposomes. *Biochim Biophys Acta Biomembr* 2003;1616:184-195.
205. Rosenfeld Y. Structure and effective interactions in multi-component hard-sphere liquids: The fundamental-measure density functional approach. *J Phys Condens Matter.* 2002;14:9141-9152.
206. Curtin WA, Ashcroft NW. Weighted-density-functional theory of inhomogeneous liquids and the freezing transition. *Phys Rev A Gen Phys.* 1985;32:2909-2919.
207. Wang DC, Gast AP. Equation of state of the hard-sphere solid: The modified weighted-density approximation with a static solid reference state. *Phys Rev E.* 1999;59:3964-3969.

208. Tarazona P. Density functional for hard sphere crystals: A fundamental measure approach. *Phys Rev Lett.* 2000;84:694-697.
209. Khein A, Ashcroft NW. Generalized density functional theory. *Phys Rev Lett.* 1997;78:3346-3349.
210. Curtin WA, Ashcroft NW. Density-functional theory and freezing of simple liquids. *Phys Rev Lett.* 1986;56:2775-2778.
211. Laird BB, Mccoy JD, Haymet ADJ. Density functional theory of freezing—Analysis of crystal density. *J Chem Phys*. 1987;87:5449-5456.
212. Groh B, Dietrich S. Crystal structures and freezing of dipolar fluids. *Phys Rev E*. 2001;6302:021203.
213. Groh B, Dietrich S. Density-functional theory for the freezing of Stockmayer fluids. *Phys Rev E.* 1996;54:1687-1697.
214. Groh B, Dietrich S. Orientational order in dipolar fluids consisting of nonspherical hard particles. *Phys Rev E.* 1997;55:2892-2901.
215. Wang DC, Gast AP. Properties of crystallizing soft sphere systems. *J Phys Condens Matter.* 1999;11:10133-10141.
216. Wang DC, Gast AP. Crystallization of power-law fluids: A modified weighted density approximation model with a solid reference state. *J Chem Phys*. 1999;110:2522-2528.
217. Wang DC, Gast AP. Crystallization of a Yukawa fluid via a modified weighted density approximation with a solid reference state. *J Chem Phys*. 2000;112:2826-2833.
218. Wang GF, Lai SK. Liquid–glass transition phase boundary for monodisperse charge-stabilized colloids in the presence of an electrolyte. *Phys Rev Lett.* 1999;82:3645-3648.
219. Laird BB, Kroll DM. Freezing of soft spheres: A critical test for weighted-density-functional theories. *Phys Rev A.* 1990;42:4810-4819.
220. Baus M. The present status of the density-functional theory of the liquid–solid transition. *J Phys Condens Matter.* 1990;2:2111-2126.
221. Groh B, Schmidt M. Density-functional theory for structure and freezing of star polymer solutions. *J Chem Phys*. 2001;114:5450-5456.
222. Denton AR, Ashcroft NW. Weighted-density-functional theory of nonuniform fluid mixtures: Application to freezing of binary hard-sphere mixtures. *Phys Rev A.* 1990;42:7312-7328.
223. Ruiz G, Tejero CF. Modified weighted density approximation for binary hard-sphere solid mixtures. *Phys Rev E.* 1998;58:5171-5174.
224. Eldridge MD, Madden PA, Frenkel D. Entropy-driven formation of a superlattice in a hard-sphere binary mixture. *Nature.* 1993;365:35-37.
225. Ohnesorge R, Lowen H, Wagner H. Density-functional theory of crystal fluid interfaces and surface melting. *Phys Rev E.* 1994;50:4801-4809.
226. Marr DWM, Gast AP. A density-functional approach to investigation of solid–fluid interfacial properties. *Chem Appl Density Funct Theory.* 1996;629:229-245.
227. Imperio A, Reatto L. A bidimensional fluid system with competing interactions: Spontaneous and induced pattern formation. *J Phys Condens Matter.* 2004;16:S3769-S3789.
228. Gotze IO, Brader JM, Schmidt M, Lowen H. Laser-induced condensation in colloid–polymer mixtures. *Mol Phys.* 2003;101:1651-1658.
229. Lowen H. Density functional theory of inhomogeneous classical fluids: Recent developments and new perspectives. *J Phys Condens Matter.* 2002;14:11897-11905.
230. Chakrabarti J, Krishnamurthy HR, Sood AK. Density-functional theory of laser-induced freezing in colloidal suspensions. *Phys Rev Lett.* 1994;73:2923-2926.
231. Rasmussen LL, Oxtoby DW. Induced freezing and re-entrant melting in the hard-disc fluid; applications of the fundamental measure functional. *J Phys Condens Matter.* 2002;14:12021-12030.
232. Lekkerkerker HNW, Coulon P, Vanderhaegen R, Deblieck R. On the isotropic–liquid crystal phase-separation in a solution of rodlike particles of different lengths. *J Chem Phys*. 1984;80:3427-3433.
233. Speranza A, Sollich P. Simplified Onsager theory for isotropic–nematic phase equilibria of length polydisperse hard rods. *J Chem Phys*. 2002;117:5421-5436.
234. Parsons JD. Nematic ordering in a system of rods. *Phys Rev A.* 1979;19:1225-1230.
235. Lee SD. A numerical investigation of nematic ordering based on a simple hard-rod model. *J Chem Phys*. 1987;87:4972-4974.
236. Varga S, Galindo A, Jackson G. Phase behavior of symmetric rod-plate mixtures revisited: Biaxiality versus demixing. *J Chem Phys*. 2002;117:10412-10424.
237. Gelbart WM, Baron BA. Generalized van der Waals theory of isotropic–nematic phase-transition. *J Chem Phys*. 1977;66:207-213.
238. ten Bosch A. Mesoscopic modeling of liquids in materials science. *Phys Chem Liquids* 2003;41:441-474.
239. Cinacchi G, Schmid F. Density functional for anisotropic fluids. *J Phys Condens Matter.* 2002;14:12223-12234.
240. Somoza AM, Tarazona P. Nematic–smectic-a–smectic-C transitions in systems of parallel hard molecules. *Phys Rev Lett.* 1988;61:2566-2569.
241. Velasco E, Mederos L, Sullivan DE. Density-functional study of the nematic–isotropic interface of hard spherocylinders. *Phys Rev E.* 2002;66:021708.
242. Velasco E, Mederos L, Sullivan DE. Density-functional theory of inhomogeneous systems of hard spherocylinders. *Phys Rev E.* 2000;62:3708-3718.
243. Graf H, Lowen H. Density functional theory for hard spherocylinders: Phase transitions in the bulk and in the presence of external fields. *J Phys Condens Matter.* 1999;11:1435-1452.
244. Cinacchi G, Mederos L, Velasco E. Liquid-crystal phase diagrams of binary mixtures of hard spherocylinders. *J Chem Phys*. 2004;121:3854-3863.
245. Bier M, Harnau L, Dietrich S. Bulk and interfacial properties of binary hard-platelet fluids. *Phys Rev E.* 2004;69:021506.
246. Velasco E, Mederos L. A theory for the liquid-crystalline phase behavior of the Gay–Berne model. *J Chem Phys*. 1998;109:2361-2370.
247. Coussaert T, Baus M. Density-functional theory of the columnar phase of discotic Gay–Berne molecules. *J Chem Phys*. 2002;116:7744-7751.
248. Varga S, Szalai I, Liszi J, Jackson G. A study of orientational ordering in a fluid of dipolar Gay–Berne molecules using density-functional theory. *J Chem Phys*. 2002;116:9107-9119.
249. Harnau L, Penna F, Dietrich S. Colloidal hard-rod fluids near geometrically structured substrates. *Phys Rev E*. 2004;70:021505.
250. Yokoyama H. Interfaces and thin fims. In: Collings P, Patel JS, eds. *Handbook of Liquid Crystal Research.* New York, NY: Oxford Univ. Press; 1997:179-235.
251. Boamfa MI, Kim MW, Maan JC, Rasing T. Observation of surface and bulk phase transitions in nematic liquid crystals. *Nature.* 2003;421:149-152.
252. Bates FS, Fredrickson GH. Block copolymer thermodynamics—Theory and experiment. *Annu Rev Phys Chem.* 1990;41:525-557.
253. Frischknecht AL, Curro JG, Frink LJD. Density functional theory for inhomogeneous polymer systems. II. Application to block copolymer thin films. *J Chem Phys*. 2002;117:10398-10411.
254. Nath SK, Nealey PF, de Pablo JJ. Density functional theory of molecular structure for thin diblock copolymer films on chemically heterogeneous surfaces. *J Chem Phys*. 1999;110:7483-7490.
255. Hamley IW. Nanostructure fabrication using block copolymers. *Nanotechnology.* 2003;14:R39-R54.
256. Park C, Yoon J, Thomas EL. Enabling nanotechnology with self assembled block copolymer patterns. *Polymer.* 2003;44:6725-6760.
257. Forster S, Antonietti M. Amphiphilic block copolymers in structure-controlled nanomaterial hybrids. *Adv Mater*. 1998;10:195.
258. Thompson RB, Ginzburg VV, Matsen MW, Balazs AC. Predicting the mesophases of copolymer-nanoparticle composites. *Science.* 2001;292:2469-2472.
259. Lee JY, Shou Z, Balazs AC. Modeling the self-assembly of copolymer–nanoparticle mixtures confined between solid surfaces. *Phys Rev Lett*. 2003;91.
260. Balazs AC. Predicting the morphology of nanostructured composites. *Curr Opin Solid State Mater Sci.* 2003;7:27-33.
261. Tanford C. *The Hydrophobic Effect: Formation of Micelles and Biological Membranes.* New York, NY: Wiley, 1980.
262. Nagarajan R, Ruckenstein E. Self-assembled systems. In: Sengers JV, ed. *Equations of State for Fluids and Fluid Mixtures.* Amsterdam, The Netherlands: Elsevier; 2000.
263. Israelachvili JN. *Intermolecular and Surface Forces.* 2nd Edition. London, UK: Academic Press; 1992.
264. Mulqueen M, Blankschtein D. Molecular-thermodynamic prediction of critical micelle concentrations of commercial surfactants. *Langmuir.* 2001;17:5801-5812.
265. Pollard ML, Radke CJ. Density-functional modeling of structure and

forces in thin micellar liquid-films. *J Chem Phys*. 1994;101:6979-6991.
266. Somoza AM, Chacon E, Mederos L, Tarazona P. A model for membranes, vesicles and micelles in amphiphilic systems. *J Phys Condens Matter.* 1995;7:5753-5776.
267. Duque D, Tarazona P, Chacon E. Microscopic model for mixed surfactant vesicles. *Langmuir.* 1998;14:6827-6834.
268. Christopher PS, Oxtoby DW. Density functional model of surfactant mesostructures. *J Chem Phys*. 2002;117:9502-9509.
269. Christopher PS, Oxtoby DW. Classical density functional study of multisite amphiphile mesostructures. *J Chem Phys*. 2003;119:10330-10338.
270. Talanquer V, Oxtoby DW. A density-functional approach to nucleation in micellar solutions. *J Chem Phys*. 2000;113:7013-7021.
271. Talanquer V, Oxtoby DW. Nucleation of pores in amphiphile bilayers. *J Chem Phys*. 2003;118:872-877.
272. Frink LJD, Frischknecht AL. Coarse grained lipids. I: A density functional approach and thermodynamics of fluid bilayers. *Biophys J.* 2005; submitted.
273. Binder K, Muller M, Virnau P, MacDowell LG. Polymer + solvent systems: Phase diagrams, interface free energies, nucleation. *Adv Polym Sci.* 2005;173:1-110.
274. Konig PM, Bryk P, Mecke K, Roth R. Curvature expansion of density profiles. *Europhys Lett.* 2005;69:832-838.
275. Kusaka I, Wang ZG, Seinfeld JH. Ion-induced nucleation—A density functional approach. *J Chem Phys.* 1995;102:913-924.
276. Elliott R, Katsov K, Schick M, Szleifer I. Phase separation of saturated and mono-unsaturated lipids as determined from a microscopic model. *J Chem Phys*. 2005;122:044904.
277. Duque D, Li XJ, Katsov K, Schick M. Molecular theory of hydrophobic mismatch between lipids and peptides. *J Chem Phys.* 2002; 116:10478-10484.
278. Yu YX, Wu JZ. Extended test-particle method for predicting the inter- and intramolecular correlation functions of polymeric fluids. *J Chem Phys.* 2003;118:3835-3842.
279. Yethiraj A, Fynewever H, Chwen-Yang S. Density functional theory for pair correlation functions in polymeric liquids. *J Chem Phys.* 2001;114:4323-4330.
280. Muller M, MacDowell LG. Wetting of a short chain liquid on a brush: First-order and critical wetting transitions. *Europhys Lett.* 2001;55: 221-227.
281. Huang DM, Chandler D. Cavity formation and the drying transition in the Lennard–Jones fluid. *Phys Rev E.* 2000;61:1501-1506.
282. Hud NV, Downing KH. Cryoelectron microscopy of λ-phage DNA condensates in vitreous ice: The fine structure of DNA toroids. *Proc Natl Acad Sci USA.* 2001;98:14925-14930.

Manuscript received Jun. 27, 2005, and revision received Sept. 10, 2005.